Surface processes and drivers of the snow water stable isotopic composition at Dome C, East Antarctica – a multi-datasets and modelling analysis

Inès Ollivier[1,2], Hans Christian Steen-Larsen[1], Barbara Stenni[3], Laurent Arnaud[4], Mathieu Casado[2],

5   Alexandre Cauquoin[5], Giuliano Dreossi[3], Christophe Genthon[6], Bénédicte Minster[2], Ghislain Picard[4],

Martin Werner[7] and Amaëlle Landais[2]

[1]Geophysical Institute, University of Bergen, and Bjerknes Centre for Climate Research, Bergen, Norway
[2]Laboratoire des Sciences du Climat et de l'Environnement, LSCE/IPSL, CEA-CNRS-UVSQ, Université Paris-Saclay, Gif sur Yvette, France
10 [3]Department of Environmental Sciences, Informatics and Statistics, Ca' Foscari University of Venice, Mestre Venice, Italy
[4]Université Grenoble Alpes, CNRS, INRAE, IRD, Grenoble INP, IGE, Grenoble, France
[5]Institute of Industrial Science, The University of Tokyo, Kashiwa, Japan
[6]Laboratoire de Météorologie Dynamique, LMD/IPSL, Sorbonne Université-CNRS, Paris, France
[7]Alfred Wegner Institute (AWI), Helmholtz Centre for Polar and Marine Research, Bremerhaven, Germany

15 *Correspondence to*: Inès Ollivier (ines.ollivier@uib.no)

Abstract. Water stable isotope records in polar ice cores have been largely used to reconstruct past local temperatures and other climatic information such as evaporative source region conditions of the precipitation reaching the ice core sites. However, recent studies have identified post-depositional processes taking place at the ice sheet's surface modifying the original precipitation signal and challenging the traditional interpretation of ice core isotopic records. In this study, we use a

20   combination of existing and new datasets of the precipitation, snow surface and subsurface isotopic compositions (δ^{18}O and d-excess), meteorological parameters, ERA5 reanalyses, outputs from the isotope-enabled climate model ECHAM6-wiso, and a simple modelling approach to investigate the transfer function of water stable isotopes from precipitation to the snow surface and subsurface at Dome C, in East Antarctica. We first show that water vapor fluxes at the surface of the ice sheet result in a net annual sublimation of snow, from 3.1 to 3.7 mm water equivalent per year between 2018 and 2020,

25   corresponding to 12 to 15% of the annual surface mass balance. We find that the precipitation isotopic signal cannot fully explain the mean, nor the variability of the isotopic composition observed in the snow, from annual to intra-monthly timescales. We observe that the mean effect of post-depositional processes over the study period enriches the snow surface in δ^{18}O by 3.3‰ to 6.6‰ and lowers the snow surface d-excess by 3.5‰ to 7.6‰ compared to the incoming precipitation isotopic signal. We also show that the mean isotopic composition of the subsurface snow is not statistically different from

30   that of the surface snow, indicating the preservation of the mean isotopic composition of the surface snow in the top centimetres of the snowpack. This study confirms previous findings about the complex interpretation of the water stable

isotopic signal in the snow and provides the first quantitative estimation of the impact of post-depositional processes on the snow isotopic composition at Dome C, a crucial step for the accurate interpretation of isotopic records from ice cores.

1 Introduction

35   Polar ice cores have been widely used in paleoclimate studies to reconstruct past atmospheric conditions, up to 800 000 years back in time (EPICA community members 2004). Within the ice matrix of the core, $\delta^{18}O$ and δD (Craig, 1961) measurements have been commonly used as a proxy for past atmospheric temperatures based on the observed relationships between the local atmospheric temperature and both the isotopic composition of precipitation samples (Dansgaard, 1964) and the snow across spatial transects in Antarctica (Lorius et al., 1969, Masson-Delmotte et al., 2008).

40   The second order parameter deuterium excess (d-excess), defined as the deviation from the existing linear relationship between $\delta^{18}O$ and δD (d-excess = $\delta D - 8 \times \delta^{18}O$, Dansgaard, 1964), is driven by physical processes involving non-equilibrium, or kinetic fractionation of the different isotopes. The d-excess measured in ice cores has been interpreted as a proxy for moisture origin (Masson-Delmotte et al., 2005) and conditions at the moisture source region, such as sea-surface temperatures and relative humidity above the ocean's surface (Merlivat and Jouzel, 1979; Jouzel et al., 1982; Vimeux et al.,

45   1999; Stenni et al., 2001; Uemura et al., 2008, 2012; Landais et al., 2021; Steen-Larsen et al., 2014a). Further kinetic processes along the distillation path of an air mass have been identified to contribute to the d-excess signal in precipitation, such as condensation in supersaturated conditions (Jouzel and Merlivat, 1984) or mixing of air masses from different origins (Risi et al., 2013).

50   The reconstruction of the climatic parameters from the water isotopic records in polar ice cores relies on the assumption that the isotopic composition of precipitation is preserved from snowfall to burial and transformation into ice. However, this has been challenged by recent field studies highlighting the significant role of post-depositional processes at the surface of both the Greenland and Antarctic ice sheets modifying the isotopic composition of precipitation after snowfall (Touzeau et al., 2016; Münch et al., 2017; Casado et al., 2018, 2021b; Hughes et al., 2021; Wahl et al., 2021, 2022; Zuhr et al., 2023). The

55   post-depositional processes commonly proposed to affect the water isotopes at the ice sheet's surface include (i) water vapor exchanges between the snow and the lower atmosphere through sublimation and condensation cycles, (ii) wind redistribution and (iii) diffusion of water vapor within the snowpack.

On the Greenland Ice Sheet, Steen-Larsen et al. (2014b) provided the first evidence of a co-variation of the snow surface and the low atmosphere water vapor isotopic compositions during precipitation-free periods in the summertime, suggesting

60   seasonal vapor exchanges between the snow and the atmosphere. Wahl et al. (2021) later measured a depleted sublimation humidity flux compared to the snow surface, showing that fractionation of water isotopes was taking place during sublimation. Including fractionation during sublimation in a simple model also improved the prediction of the day-to-day variability in the snow isotopic composition during summertime (Wahl et al., 2022). Additional laboratory and modelling

studies showed that sublimation leads to an enrichment in $\delta^{18}O$ together with a lowering of d-excess in the surface snow and
in the firn (Hughes et al., 2021; Dietrich et al., 2023).

In addition, diffusion of water vapor within the snowpack is driven by temperature and isotopic gradients and affects the
isotopic composition of the snow and firn continuously (Johnsen et al., 2000; Gkinis et al., 2014). Field studies on both the
Greenland and Antarctic Ice Sheets identified snow metamorphism associated with water vapor diffusion within the top
layers of the snow to affect the snow isotopic composition ($\delta^{18}O$ and d-excess) after snowfall (Casado et al., 2021b; Harris
Stuart et al., 2023).

Lastly, the wind blowing at the surface of the ice sheet leads to a heterogeneous accumulation by redistributing the snow on
the surface (Libois et al., 2014; Picard et al., 2019; Zuhr et al., 2021) which impacts the build-up of the isotopic signal in the
snow (Zuhr et al., 2023). Wind is also hypothesized to impact the snowpack isotopic composition through forced pumping
and ventilation of the snowpack (Town et al., 2008).

At Dome C, on the East Antarctic Plateau, previous studies have focused on qualitative description of the impact of post-
depositional processes on the snow surface at Dome C (Casado et al., 2018), monitoring the atmospheric water vapor,
surface snow and precipitation isotopic compositions (Casado et al., 2016; Touzeau et al., 2016; Stenni et al., 2016; Dreossi
et al., 2023) or exploring the isotopic signature of snow metamorphism (Casado et al., 2021b). However, a comprehensive
understanding of the formation of the isotopic signal in the snow, is still missing.

In this study we address the transfer function of water stable isotopes from precipitation to the snow surface and subsurface
at Dome C, from intra-monthly to multi-annual timescales. We use a combination of existing and new datasets of the
isotopic composition of precipitation, surface snow and subsurface snow over five consecutive years (2017-2021), ERA5
reanalysis products, outputs from the isotope-enabled climate model ECHAM6-wiso and a simple modelling approach to
investigate the contribution of precipitation to the variability observed in the snow surface and subsurface isotopic
composition. In addition, we use the meteorological parameters measured continuously on-site to estimate the magnitude of
sublimation and condensation fluxes between the surface and the lower atmosphere over three consecutive years (2018-
2020) and qualitatively evaluate their impact on the snow isotopic composition at Dome C.

2 Data and methods

2.1 Geographical settings

Dome C is located on the East Antarctic Plateau (75.1°S, 123.3°E), at 3233 m a.s.l. and 1000 km from the coast and is the
site where the permanent research station Concordia is installed (see location on Fig. 1a). The site is characterized by a mean
annual temperature of about -52°C (Genthon et al., 2021a) and a low accumulation rate of about 2.5 cm w.e. year^{-1} (Genthon
et al., 2015). Due to the very small local slope and the location on a dome, the site is not subjected to strong katabatic winds,
the mean annual wind speed close to the surface is about 4 m s^{-1} (Genthon et al., 2021a).
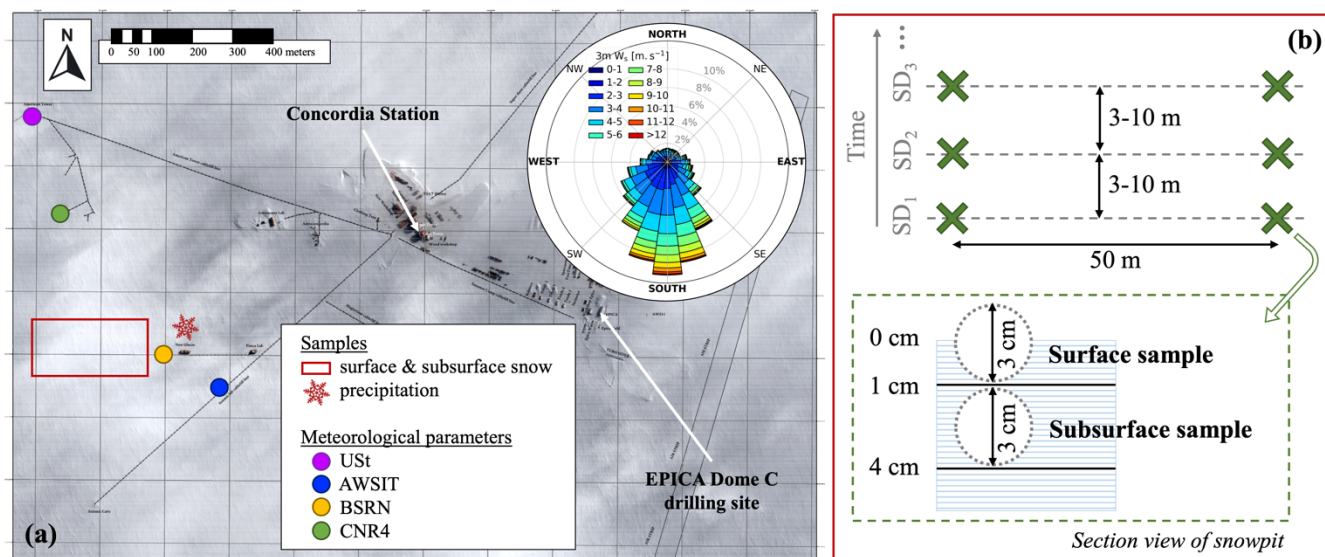
3

Figure 1. (a) Aerial view of Concordia station. The coloured circles indicate the location of the meteorological measurements used in this study (Sect. 2.4) and in red (rectangle and snowflake) the location of the samples presented in this study (Sect. 2.2 and 2.3). The wind rose for the five-year period 2017-2021 of the wind at 3 m is shown in the upper right corner. Background image from CNES (Pléiade satellite image of Concordia Station, Antarctica, CNES 2016, Distribution Airbus Defence and Space). (b) Snow sampling scheme taking place in the red rectangle in panel (a) (described in Sect. 2.2). SD stands for sampling day.

2.2 Snow surface and subsurface sampling

The regular sampling of the top few centimetres of the snow started in November 2013 and the sampling of a subsurface layer was added in 2017. Since then, the sampling strategy remained the same. In this study we focus on the 5-year period 2017-2021, where both surface and subsurface samples are available for analysis (see also Table 1).

The sampling takes place in the clean area about 800 m upwind of the main buildings (see location on Fig. 1a), twice a week and all-year round. The samples are taken at two different locations 50 m apart along a straight line, 3 to 10 m next to the line of the previous sampling day. At each location along the line, a small vertical snowpit is dug (about 20 cm deep). The snow surface and subsurface are collected with two 50 mL Corning tubes, placed horizontally from the snowpit wall, at the surface and just below. The two snow samples correspond to depths of 0 to 1 cm deep for the surface sample and from 1 to 4 cm for the subsurface sample, although the exact sampling depths was not recorded and may have slightly varied with the change of operator throughout the years or within one year due for instance to hard snow. The sampling scheme is illustrated in Fig. 1b.

Once the snow samples are collected, the tubes are sealed to prevent air exchange with the surrounding atmosphere and stored at temperatures well below freezing. The samples are shipped back once a year to LSCE (CNRS Paris-Saclay) to measure their isotopic composition with a laser spectrometer PICARRO L2130-i in liquid mode. We report the snow isotopic composition with delta-notation in ‰ (Craig, 1961) with respect to the Vienna Standard Mean Ocean Water

(VSMOW) (Gonfiantini, 1978). The associated uncertainty (two standard deviation of sample replicates) on these measurements is $\pm$ 0.2‰ for δ^{18}O and $\pm$ 0.7‰ for δD.

120

The 5-year compiled dataset of the snow surface and subsurface isotopic composition used in this study is in (dataset in review with PANGAEA). Part of this dataset was published in Casado et al. (2021a), with an overlap with this study from January 2017 to April 2018 for the surface snow samples.

2.3 Precipitation sampling

125   Since 2008, precipitation samples have been collected in the vicinity of Concordia station, as part of different projects operated by the Italian Antarctic Research Programme (PNRA). Part of this long time series have been published in Stenni et al. (2016) (2008-2010) and Dreossi et al. (2023) (up to 2017). Here we extend the record of the precipitation isotopic composition to 2021 and use the timeseries from 2017 to 2021 for our analysis (see also Table 1). The new dataset (2018-2021) is available in PANGAEA (dataset in review with PANGAEA).

130   Precipitation samples are collected every day on a wooden platform (bench) 1 m above the ground, covered by a PTFE surface and shielded by an 8 cm rail. The bench is situated about 800 m upwind of the main buildings (see location in Fig. 1a). The samples are collected at 10 AM local time (UTC+8), although it has varied throughout the years depending on the operator. All the snow laying on the bench is collected, whether it is precipitation (including diamond dust), blown snow or air hoar from atmospheric condensation. It cannot be ruled out that some of the samples might have undergone sublimation
135   especially during the summertime, because of exposure to 24-hour solar radiation before sample collection (Stenni et al., 2016; Dreossi et al., 2023). Each precipitation sample collected is weighted, and we use these weights as approximate estimates of the precipitation amounts (details in Sect. 2.5).

After collection, the plastic bag containing the sample is sealed and stored at temperatures well below freezing before annual shipment to the Ca'Foscari University of Venice, Italy, where the isotopic composition of the samples is measured with a
140   PICARRO laser spectrometers (L2130-i and L2140-i). We report the snow isotopic composition with delta-notation in ‰ (Craig, 1961) with respect to the Vienna Standard Mean Ocean Water (VSMOW) (Gonfiantini, 1978). The associated uncertainty (one standard deviation of quality standard replicates) on these measurements is $\pm$ 0.08‰ for δ^{18}O and $\pm$ 0.68‰ for δD.

2.4 Meteorological parameters

145   ### 2.4.1 Atmospheric monitoring

Atmospheric parameters are measured continuously at Dome C by different weather stations and instruments installed nearby Concordia station. For the 2017-2021 period of interest of this study, we used meteorological observations both from

an Automatic Weather Station operated by the PNRA (referred as AWSIT hereinafter) and from a 42 m meteorological tower (referred as USt hereinafter). A summary of the meteorological parameters used in this study is available in Table 1.

150   The AWSIT is located about 800 m upwind of Concordia station (see location in Fig. 1a) and has been operating since 2005. The data are available at 1 hour time step (1-hour averages) in Grigioni et al. (2022). In this study, we use the atmospheric pressure measured at 1 m above the surface with a Vaisala PTB100 and a 3-month period of the atmospheric temperature measured at 1.5 m by a Vaisala HMP45D. To match the same time step of the observations from the USt described below, we linearly interpolated the data to 30 min.

155   The USt is part of the CALVA project and located about 1 km of Concordia station (see location in Fig. 1a). Meteorological instruments are installed at six different levels in the atmosphere measuring continuously for more than ten years (Genthon et al., 2021a). Due to snow accumulation, the sensors installed on the lowest level of the tower, at 3 m above the surface, were 40 cm closer to the surface in 2021 than in 2017. This height change was not considered here, and the lowest level of the tower is referred to as the 3 m level. All atmospheric parameters are sampled at 30 s intervals, however in this study we use

160   the 30 min averages.

The atmospheric temperature is measured by a PT100 in a Vaisala HMP155 combined sensor (thermohygrometer) placed in a mechanically aspirated shield (Young 43502) and the wind speed and direction are measured by Young 05103 aerovanes. The quality-controlled (QC) data for temperature and wind speed from 2010 to 2019 is available in Genthon et al. (2021b, c). Here we use this dataset from 2017 to 2019 and extend the record up to 2021 using the data from the same instruments

165   available on the CALVA project website (see Table 1). Since the quality-control of this additional period (2019-2021, referred as non-QC) is not guaranteed, we compared the QC and non-QC datasets during an overlapping period (not shown). We found no significant difference and therefore use the temperature and wind records from the USt between 2017 and 2021 in our analysis. Note that to fill a 3-month period of missing temperature data from the USt in 2021 (August to October), we use the temperature measured by the AWSIT (described above). There was no significant difference between the two

170   temperature records during overlapping periods (not shown). The mean temperature and wind speed over the period 2017-2021 are summarized in Table 1. The dominant wind direction over the same period is shown in the windrose in Fig. 1a.

Atmospheric water vapor content (or humidity) is also measured continuously by sensors installed on the meteorological tower. At Dome C, the surface atmosphere is very cold and frequently above saturation (Genthon et al., 2017), and in these conditions the standard humidity sensors fail to accurately measure the true atmospheric humidity content. To cope with this

175   issue, a modified HMP155 was designed and installed on the USt at 3 m above the ground, and proved its utility to measure atmospheric moisture accurately, capture supersaturation conditions and expand the temperature operating range of the humidity sensor (Genthon et al., 2017, 2022). The sensor reports atmospheric humidity with respect to liquid (RH_{wrtl}) water even at temperature below 0°C, we therefore convert RH_{wrtl} to the relative humidity with respect to ice (RH_{wrti}), as in Genthon et al. (2017) and Vignon et al. (2022) (see also Supplement S1). The relative humidity at 3 m in the atmosphere and

180   at 30 min resolution over the 2018-2021 period is available in Genthon et al. (2021d) and an analysis of the dataset is available in Genthon et al. (2022). Vignon et al. (2022) further provides estimations of the uncertainties for RH_{wrti} associated

with the temperature and humidity measurements. In this study, we use this 3-year atmospheric humidity record to estimate water vapor fluxes at the snow surface. The method is described in the following section. The mean RH_{wrti} between 2018 and 2020 is indicated in Table 1.

185

Table 1. Summary of samples and meteorological parameters used in this study and the reference to the data. The average values for temperature and wind speed are calculated over the 2017-2021 period; the relative humidity with respect to ice, the atmospheric pressure and the surface temperature are calculated over 2018-2020. The CALVA project website is accessible at: https://web.lmd.jussieu.fr/~cgenthon/SiteCALVA/CalvaData.html. The CNR4 (*) data will be published upon acceptance of the article.

Project	Type/depth or height	Sampling rate/measurement time step	Average	Reference to dataset
NIVO	Snow samples: surface (0-1 cm) and subsurface (1-4 cm)	2x / week	–	Casado et al., (2021a) & this study
PRE-REC/ WHETSTONE	Precipitation samples	daily	–	Dreossi (2023) & this study
CALVA (USt)	3 m temperature	30 min	-52.1°C	Genthon et al. (2021b) & CALVA website (see Table caption)
CALVA (USt)	3 m wind speed	30 min	3.9 m s^{-1}	Genthon et al. (2021c) & CALVA website (see Table caption)
CALVA (USt)	3 m RH_{wrti}	30 min	104.5%	Genthon et al. (2021d)
AMCO (AWSIT)	Pressure at 1 m	1 h	642.6 hPa	Grigioni et al. (2022)
NIVO (CNR4)	Surface temperature	10 min	-55.4°C	* see Table caption

2.4.1 Estimation of water vapor fluxes

190

During the period of interest of this study, no direct Eddy-Covariance (EC) fluxes measurements were available at Dome C. We instead make use of the standard atmospheric parameters measured on site (described in the previous section) to apply the bulk method as described in Genthon et al. (2017) and estimate water vapor fluxes between the surface and the 3 m atmospheric level. We report the 30 min averages vapor fluxes during the 3-year period 2018-2020 in mm water equivalent per timestep.

195

The bulk method is based on the Monin-Obukhov (MO) Similarity Theory (Monin and Obukhov, 1954) and relies on several assumptions, which may not hold over the Antarctic Plateau (Vignon et al., 2016). Nevertheless, this method is still commonly used as the parametrization of surface turbulent fluxes in global and regional climate models (e.g. MAR model, Gallée and Schayes 1994) and have been compared against Eddy-Covariance measurements both at Dome C on the East

200

Antarctic Ice Sheet (sensible heat fluxes, Vignon et al., 2016) and at EastGRIP on the Greenland Ice Sheet (water vapor fluxes, Dietrich et al., 2024). It requires the following parametrizations: (1) the choice of roughness length for momentum (z_0), (2) the choice of functions representing the atmospheric stability and (3) the calculation of the roughness lengths for water vapor (z_{0q}) and heat (z_{0t}). In their sensitivity study on the parametrization for sensible heat flux estimations at Dome C, Vignon et al. (2016) recommend the use of the stability functions from Holtslag and De Bruin (1988, referred hereinafter as

205 H88) for stable cases and the functions from Högström (1996) for unstable cases. They also recommend the use of a constant z_0 of 0.56 mm, which corresponds to the average value observed with an EC system over one year at Dome C (Vignon et al., 2016). For the parametrization of z_{0q} and z_{0t}, we use the same approach as in Genthon et al. (2017) and King et al. (2001) where $z_0 = z_{0q} = z_{0t}$. We used this parametrization (H88, $z_0 = z_{0q} = z_{0t} = 0.56 \times 10^{-3}$ m) as the reference parametrization. In addition, and similarly as in Vignon et al. (2016) and Genthon et al. (2017), we computed the water vapor fluxes using three

210 other stability functions for stable conditions and a range of z_0 to estimate the sensitivity of the final flux calculations on the parametrization (fluxes computed 16 times, see Table 2 for stability functions and range of z_0). The range of z_0 tested corresponds to the observed range over one year at Dome C (Vignon et al., 2016).

Table 2. Set of roughness lengths for momentum z_0 and stability functions for stable conditions used to compute water vapor fluxes with
215 the bulk method. The reference parametrization is highlighted in bold.

Roughness length for momentum z_0	0.01×10^{-3} m
	0.56×10^{-3} m
	1×10^{-3} m
	6.3×10^{-3} m
Stability function for stable conditions	**Holtslag and De Bruin (1988) – H88**
	Lettau (1979)
	Grachev et al. (2007)
	King and Anderson (1994)

To compute the water vapor fluxes, the bulk method requires temperature, wind speed, specific humidity, and pressure at the chosen atmospheric level (3 m here), as well as the snow surface temperature and the specific humidity at the surface.

220 For the atmospheric level, we use the temperature, wind and humidity sensors installed at 3 m above the surface on the USt together with the atmospheric pressure measured by the AWSIT (measurements described in Sect. 2.4.1). The formulas from Murphy and Koop (2005) are used to convert RH_{wrti} into specific humidity. To guarantee that the stationary conditions required to apply the bulk method are met, we removed all 30 min temperature and wind speed data for which the differences in temperature and wind speed with the previous half-hour were above 2°C and 1.1 m s^{-1}, respectively (Vignon et
225 al., 2016). This represents 4% of the whole dataset.

For the surface level, the snow surface temperature is computed from upward and downward longwave radiative fluxes with the same method as in Vignon et al. (2016) (their Eq. 1), using the same snow emissivity of 0.99 (value given by Brun et al., 2011, used in Vignon et al., 2016 and Genthon et al., 2017). We use the longwave radiative measurements from a CNR4 radiometer installed approximately 500 m away from the USt (see location in Fig. 1a). We average the data over 30 min to
230 match the time resolution of the atmospheric measurements (originally 10-min resolution). Note that to fill a 3-month period of missing data in the CNR4 record at the end 2020, we use the data provided by the BSRN network (Lupi et al., 2021). The BSRN data was corrected on the CNR4 data during overlapping periods beforehand, due to a shift identified in the upward longwave flux measured by the BSRN pyrgeometer from December 2019 onwards. The mean surface temperature over the

2018-2021 time-period is reported in Table 1. The specific humidity at the snow surface is converted from the surface

235 temperature using the formulas from Murphy and Koop (2005) and assuming saturation.

In total, due to gaps in the different input datasets and the removal of non-stationary data, the missing data in the bulk estimations represents 9% of the whole dataset.

2.5 Snow Isotopic Signal Generator (SISG)

To evaluate the contribution of precipitation to the isotopic variability observed in the snow surface and subsurface samples

240 collected at Dome C (described in Sect. 2.2), we use a simple modelling approach to create synthetic snow layers solely based on the incoming precipitation. This approach was used in Casado et al. (2018, 2021b) for a similar purpose, but focused on the top layer of the snowpack. Here we re-implemented the same simple model and added the subsurface snow.

The model (referred to as the Snow Isotopic Signal Generator – SISG) simulates snow layers by stacking precipitation events until the thickness of the stacked precipitation reaches the depths of the snow surface and subsurface layers given as input of

245 the model. The isotopic composition of each snow layer is then calculated as the weighted average (by precipitation amounts) isotopic composition of all precipitation events necessary to build the snow layers. We choose the input snow layers depths to be 0 to 1 cm for the surface layer and 1 to 4 cm for the subsurface layer to match the snow samples collected at Dome C. We run the model at daily resolution over the 5-year period 2017-2021 and retrieve the model results for the same days as the observations. Table 5 summarizes the five model experiments performed with different inputs for the

250 precipitation isotopic composition and precipitation amounts (described in Sect. 2.5.1 and 2.5.2).

Table 3. Experiments performed with the SISG model, with respective inputs for the daily precipitation amounts (described in Sect. 2.5.1) and the daily isotopic composition of precipitation (described in Sect. 2.5.2). Note that the precipitation amounts from the observations, ERA5 and ECHAM6-wiso are scaled to match the mean annual accumulation observed at Dome C.

255

Experiment	Daily precipitation amount	Daily precipitation isotopic composition
"Iso from T & cst accu"	Constant	Assuming constant iso vs temperature relationship
"Iso from T & ERA5 accu"	ERA5	Assuming constant iso vs temperature relationship
"Iso from wg. mm & obs accu"	Observations	Precipitation-weighted mean annual isotope cycle
"Iso from ar. mm & obs accu"	Observations	Arithmetic mean annual isotope cycle
"Iso from ECHAM6 & ECHAM6 accu"	ECHAM6-wiso	Modelled by ECHAM6-wiso

2.5.1 Daily precipitation amounts

The first SISG experiment uses a timeseries with a constant daily precipitation amount, calculated by dividing the mean annual accumulation at Dome C by 365 days. We use a mean annual accumulation of 2.5 cm w.e. year^{-1} estimated from stake measurements (Genthon et al., 2015). This corresponds to 8 cm year^{-1} using a snow density of 320 kg m^{-3}, a typical value for

260 surface snow at Dome C (Picard et al., 2014; Genthon et al., 2015; Leduc-Leballeur et al., 2017). Hereafter, we use this

9

same snow density to convert precipitation amounts from snow water equivalent (SWE in mm w.e.) to snow depths (mm of snow) and inversely.

The second experiment uses the precipitation amount timeseries from ERA5 reanalysis (Hersbach et al., 2020, dataset available in Muñoz Sabater, 2019). We use the 24h-average of the hourly snowfall rate data for the grid point nearest
265 Concordia station as an input to the model.

The third and fourth experiments use the observed precipitation amounts. As in Kopec et al. (2019), we assume that the weight of the daily precipitation samples collected on site for isotopic analysis (Sect. 2.3) is proportional to the amount of precipitation that has fallen over the day.

The fifth experiment uses the precipitation amounts given by the isotope-enabled global circulation model (GCM)
270 ECHAM6-wiso (described in Cauquoin et al., 2019). The simulation was performed at a spatial resolution of 0.9° and nudged to ERA5 reanalyses (Cauquoin and Werner, 2021). The daily precipitation amounts were extracted for the grid point closest to Dome C. The ECHAM6-wiso outputs from 1990 to 2020 are available in Cauquoin and Werner (2023), and the simulation was extended to 2021 by A. Cauquoin.

Because the cumulative sum of the precipitation amounts according to the observations, ERA5 and ECHAM6-wiso was too
275 low (18, 18, and 32 cm of snow after five years, respectively) compared to the mean accumulation over five years at Dome C (40 cm of snow), we scaled up all daily precipitation amounts in the three timeseries to match the mean annual accumulation (8 cm year^{-1}), acknowledging that this value is still underestimated because of net annual sublimation (Sect. 3.1). These scaled timeseries were used as inputs for the SISG model. The comparison of the three timeseries is shown in Fig. 5 (Sect. 3.3.1).

280 **2.5.2 Daily precipitation isotopic composition**

Due to some gaps in the daily precipitation samples collected at Dome C (described in Sect. 2.3), the timeseries of isotopic composition cannot be used as a direct input to the SISG model. Instead, we generate three artificial timeseries based on (1) the atmospheric temperature, (2) the precipitation-weighted mean annual isotope cycle in precipitation and (3) the arithmetic mean annual isotope cycle in precipitation. A comparison of these three artificial timeseries and the daily observations of the
285 precipitation isotopic composition is shown in Fig. S2 (Supplement S3.1).

The first and second SISG experiment uses the artificial timeseries based on the atmospheric temperature. The precipitation isotopic composition is calculated from the atmospheric temperature using the linear relationships between $\delta^{18}O$ and δD of the precipitation samples and the 3 m daily mean temperature (Eq. 1 and 2 in Sect. 3.3.3). Deuterium excess is then calculated from the theoretical values of $\delta^{18}O$ and δD.

290 The third SISG experiment uses an artificial timeseries where all days in each month have the same isotopic composition than the corresponding monthly precipitation-weighted mean isotopic composition calculated over five years (results presented in Sect. 3.3.2, Fig. 6c and f).

The fourth experiment uses an artificial timeseries where all days in each month have the same isotopic composition than the corresponding monthly arithmetic mean isotopic composition calculated over five years (results presented in Sect. 3.3.2, Fig. 6b and e).

The fifth experiment uses the daily precipitation isotopic composition modelled by ECHAM6-wiso. In the simulations, all data points outside of the 5-year average ± three standard deviation range were discarded (six data points for $\delta^{18}O$ and 20 data points for d-excess over five years). A comparison of the observed daily precipitation isotopic composition and ECHAM6-wiso simulations is shown in Fig. 6 (Sect. 3.3.2).

3 Results

3.1 Surface moisture fluxes

The water vapor fluxes from the surface to the lower atmosphere for the period 2018-2020 estimated using the meteorological parameters measured at Dome C and the bulk method (described in Sect. 2.4.2) are shown in Fig. 2.
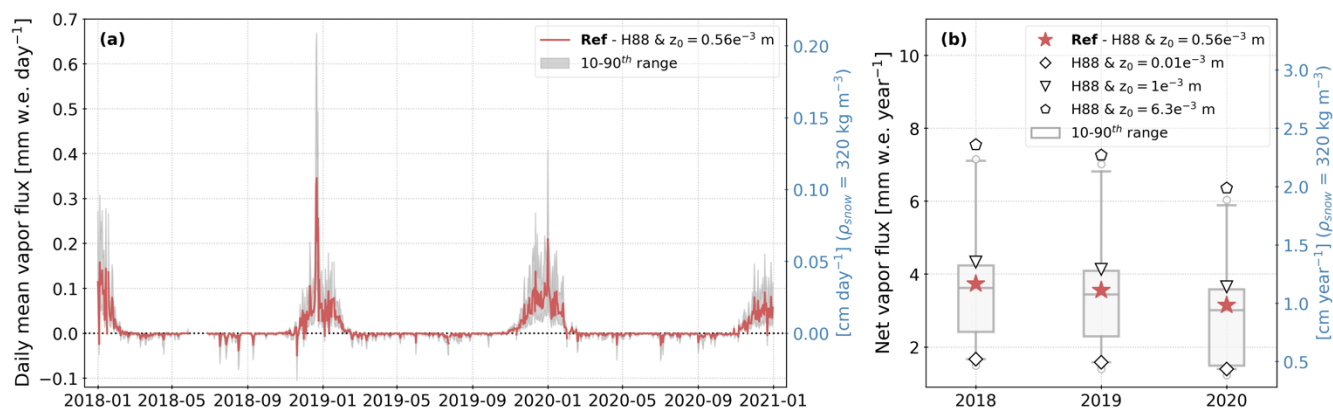
Figure 2. Water vapor fluxes at Dome C during the period 2018-2020 (positive for sublimation, negative for condensation). Panel (a) displays the 3-year timeseries of daily mean water vapor flux in mm water equivalent. The red line corresponds to the reference parametrization and the grey shading corresponds to the 10-90th percentile range of all parametrizations (described in Sect. 2.4.2). Panel (b) shows the net annual water vapor flux (sum of sublimation and condensation over one year). The red stars indicate the reference parametrization, and the three other black markers indicate the results using the stability function H88 with different z_0. The whiskers of the grey boxplots indicate the 10-90th percentile range of all parametrizations, and the grey circles indicate the outliers outside of this range. The secondary axis to the right in blue gives water vapor fluxes in cm of snow, using a snow density of 320 kg m-3 to convert SWE to snow height.

During the 3-year period 2018-2020, the daily mean water vapor flux calculated with the reference parametrization varied from -0.05 (condensation) to 0.35 (sublimation) mm water equivalent per day (red line in Fig. 2a). The seasonality of moisture fluxes over this period is characterised by sublimation during the summer months while little condensation is observed during the rest of the year. This seasonal pattern is observed independently of the parametrization used in the bulk method, which only affects the magnitude of the fluxes (grey shading in Fig. 2a).

The net annual water vapor flux between 2018 and 2020 is positive, meaning a net annual sublimation of snow, regardless of
320   which parametrization is used (grey boxplots in Fig. 2b). In 2018, 2019, and 2020, water vapor fluxes calculated with the
reference parametrization led to a net mass loss of 3.7, 3.6, and 3.1 mm w.e., respectively (red stars in Fig. 2b), which is
slightly higher than the net water vapor flux of 2.8 mm w.e. in 2015 (Genthon et al., 2017). These values correspond to 1.2,
1.1, and 1.0 cm of snow, respectively, using a snow density of 320 kg m^{-3} to convert from SWE to snow height. They are
doubled when using a roughness length for momentum of 6.3×10^{-3} m instead of 0.56×10^{-3} m (black pentagons in Fig. 2b)
325   and divided by approximately two when using a roughness length for momentum of 0.01×10^{-3} m (black triangles in Fig.
2b). The net annual water vapor fluxes are increased by 0.1 mm w.e. using a sensor height of 2 m above the surface instead
of 3 m to consider height changes of the sensors (Sect. 2.4.1). During the summer periods only (from November to February,
both months included), water vapor fluxes led to a net sublimation of 4.4, 4.1, and 3.8 mm w.e. in 2018, 2019, and 2020,
respectively (not shown).

330   **3.2 Snow isotopic composition**

3.2.1 Temporal variations over five years

The five-year timeseries of the snow surface and subsurface isotopic composition (δ^{18}O and d-excess) is displayed in Fig. 3,
together with the respective mean annual cycle (monthly means) for each layer over the whole period.
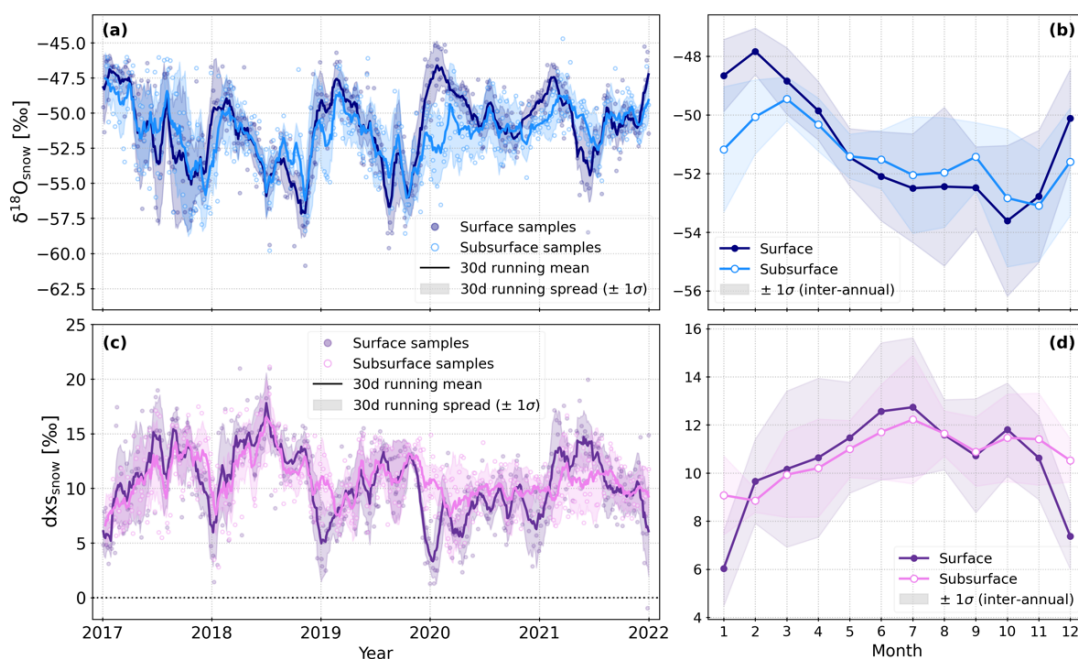

335   **Figure 3.** Observations of the surface and subsurface snow isotopic composition at Dome C. Panels (a) and (c) show the 5-year timeseries
(2017-2021) for δ^{18}O and d-excess (dxs) respectively. The circles represent the horizontal average between the two samples taken at the
two locations 50 m apart on the sampling lines (described in Sect. 2.2) and the solid lines show a 30-day running mean of these horizontal
averages. The shaded area represents the 30-day running average of the spatial spread between the two samples taken at the two locations

340 50 m apart on the sampling lines (one standard deviation). Panels (b) and (d) show the mean annual cycles (monthly means) of the surface and subsurface snow layers calculated over the period 2017-2021 for $\delta^{18}O$ and d-excess respectively. The shaded area represents the inter-annual variability around the mean annual cycle (one standard deviation). The symbols on the right vertical axis indicate the mean isotopic composition of the snow surface and subsurface layers across all years. In all four panels, the darker colours correspond to the surface samples and the lighter colours to the subsurface samples.

345 Considering all samples collected during the five-year period, the $\delta^{18}O$ in the snow has a large amplitude, with values ranging from -60.9‰ to -45.1‰ in the surface layer and from -59.8‰ to -44.7‰ in the subsurface layer (circles in Fig. 3a). Both snow layers have a higher $\delta^{18}O$ during the summertime and lower values in the wintertime (lines in Fig. 3a).

This seasonality is further visible in their respective mean annual cycles (Fig. 3b), with the surface snow $\delta^{18}O$ highest in February (-47.8‰) and lowest in October (-53.6‰, dark blue in Fig. 3b). Compared to the surface snow, the mean annual

350 cycle in the subsurface snow has a smaller amplitude and is shifted in time, with a maximum in March (-49.5‰) and a minimum in November (-53.1‰, light blue in Fig. 3b).

The temporal variation of the surface snow $\delta^{18}O$ is characterized by sharp increases during the summertime followed by slow decreases through the winter, which is particularly clear for the summers 2017-2018, 2018-2019 and 2019-2020 (dark blue line in Fig. 3a). This asymmetric seasonal pattern has been previously identified by Casado et al. (2018) for earlier years and

355 is reflected in the mean annual cycle of the surface snow $\delta^{18}O$ (dark blue in Fig. 3b). A similar pattern is visible in the subsurface snow, although with a reduced amplitude (light blue in Fig. 3a and b).

The variations of $\delta^{18}O$ in the surface and the subsurface snow generally follow each other, except for specific periods when the surface and subsurface differ by several per mill, for example at the beginning of 2020 (solid lines and shaded areas in Fig. 3a). This difference between the two snow layers is reflected in their respective mean annual cycles and is the largest

360 during the summer (Fig. 3b).

The overall mean $\delta^{18}O$ of the surface and subsurface snow is -51.0 ± 0.2‰ and -51.4 ± 0.1‰, respectively (dark and light blue dots in Fig. 3b). The uncertainty around these mean values corresponds to the standard error of the mean (SEM), calculated using the effective number of independent samples in the timeseries (Bretherton et al., 1999, Supplement S2).

365 As for $\delta^{18}O$, the surface and subsurface snow show large variations in d-excess over the five-year period (Fig. 3c). Considering all samples collected over the period, d-excess ranges from -0.9‰ to 21.0‰ in the surface snow and from 2.8‰ to 21.1‰ in the subsurface snow (dots in Fig. 3c). In opposition to $\delta^{18}O$, high d-excess values are encountered in the wintertime and lower d-excess in the summertime (lines in Fig. 3c).

This seasonality in d-excess is further reflected in the mean annual cycles of both snow layers (Fig. 3d). The surface snow d-

370 excess is the highest in July (12.7‰) and the lowest in January (6.0‰, dark purple in Fig. 3d). As for $\delta^{18}O$, the mean annual cycle in the subsurface snow has also a smaller amplitude compared to the surface layer, with a maximum in July (12.2‰) and a minimum in February (8.9‰, violet in Fig. 3d). However, contrary to $\delta^{18}O$, the mean annual cycle in the subsurface snow does not show a clear time lag compared to the surface. Instead, the variations in the subsurface follows the ones of the surface, apart from the summer months of January and December where the subsurface has larger d-excess than the surface

375 layer (Fig. 3d). This summertime difference in d-excess between the surface and subsurface layers is also visible in the timeseries, in particular during the summer 2019-2020 (Fig. 3c).

Lastly, the variations in d-excess in the surface snow do not have the same pattern as for $\delta^{18}O$ (sharp increase in summertime and slow decrease in the wintertime). Instead, the surface snow d-excess shows a more symmetric seasonal evolution than $\delta^{18}O$ (dark purple line in Fig. 3c). This symmetry is reflected in the mean annual cycle in d-excess of the surface snow (Fig.

380 3d).

The overall mean d-excess of the surface and subsurface snow is 10.4 ± 0.2‰ and 10.8 ± 0.1‰, respectively (dark purple and violet dots in Fig. 3d). The uncertainty around these mean values corresponds to the SEM, calculated the same way as for $\delta^{18}O$.

3.2.2 Vertical difference between the surface and subsurface snow

385 In the previous section, we identified a seasonal pattern in the vertical difference between the surface and subsurface snow isotopic compositions ($\delta^{18}O$ and d-excess). The vertical difference is defined here as the isotopic composition of the surface layer minus the isotopic composition of the subsurface layer.

Considering all samples collected during the five-year period (displayed as dots in Fig. 3a and c), the minimum difference in $\delta^{18}O$ between the surface and the subsurface snow is -7.5‰ (surface depleted in $\delta^{18}O$ compared to subsurface) and the

390 maximum difference is 9.1‰ (surface enriched in $\delta^{18}O$ compared to subsurface). The corresponding minimum and maximum values in the vertical difference in d-excess are -10.6‰ and 12.3‰, respectively.
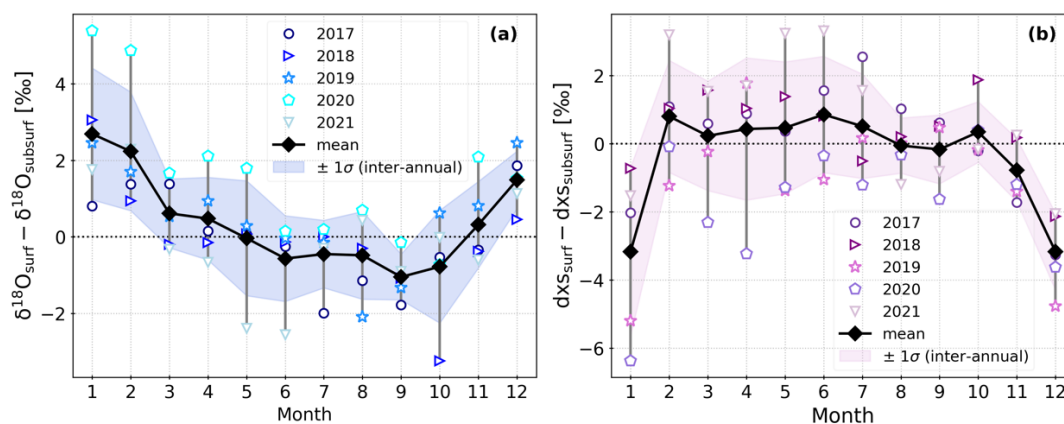
Figure 4. Mean annual cycle (monthly means) of the observed vertical difference between the snow surface and subsurface isotopic composition at Dome C. Panel (a) shows the mean annual cycle of the vertical difference in $\delta^{18}O$, panel (b) shows the mean annual cycle
395 of the vertical difference in d-excess. In both panels, the black diamonds correspond to the overall monthly means calculated over the 2017-2021 period. The shaded area shows the inter-annual variability of individual years around the overall monthly means (one standard deviation) and the coloured markers show the monthly means for each individual year.

The mean annual cycles of the vertical difference in $\delta^{18}O$ and d-excess between the two depths show a clear seasonal pattern

400 (Fig. 4a and b). The surface snow is relatively enriched in $\delta^{18}O$ from November to April and relatively depleted from May to
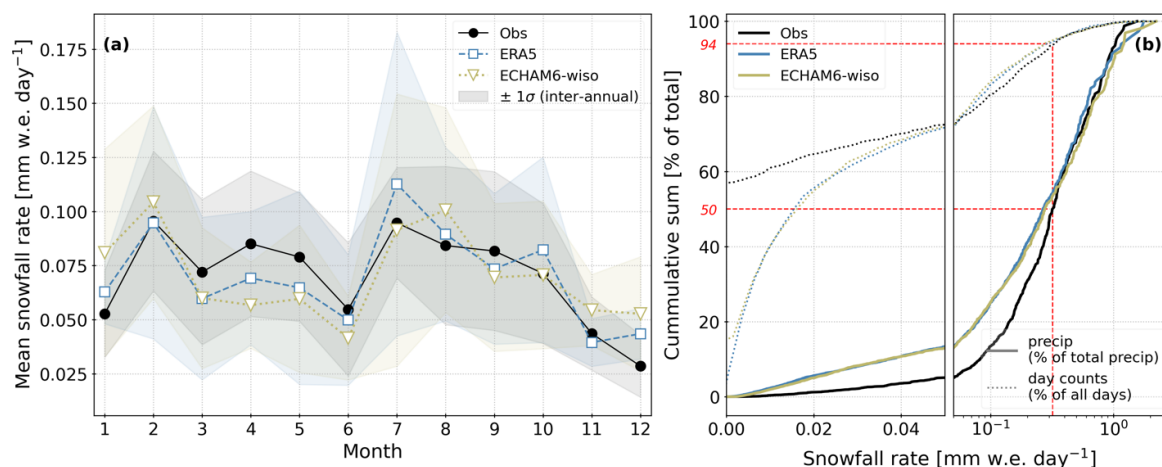
October compared to the subsurface (black diamonds in Fig. 4a). The maximum vertical difference is 2.7‰ and occurs in January, the minimum difference is -1.0‰ and occurs in September. However, compared to the inter-annual variability within the averaging period (coloured markers and shaded area in Fig. 4a), only the months of January, February, September, and December show a substantial vertical difference in $\delta^{18}O$ between the snow layers.

405 In opposition to $\delta^{18}O$, the surface snow has a lower d-excess in the summer months of January and December, with a maximum monthly mean difference of -3.2‰ in January (black diamonds in Fig. 4b). The minimum difference of 0.9‰ is found in June and is, however, negligible compared to the inter-annual variability within the averaging period (coloured markers and shaded area in Fig. 4b).

3.3 Precipitation amounts and isotopic composition in observations, ECHAM6-wiso and ERA5 reanalyses

410 ### 3.3.1 Precipitation amounts

To evaluate whether ERA5 reanalysis data and ECHAM6-wiso results correctly capture the precipitation amounts at Dome C, we compare them with the observations in Fig. 5 (all three timeseries scaled to the observed mean annual accumulation, Sect. 2.5).

Figure 5. Precipitation amounts at Dome C from observations, ERA5 reanalyses and ECHAM6-wiso simulation outputs. Panel (a) shows the mean annual cycles (monthly means) of the daily precipitation amounts (in mm w.e. per day) calculated over the period 2017-2021. Panel (b) shows the cumulative sum of precipitation over 5 years, reported as percentage of the total amount of precipitation (black and coloured thick lines), and the cumulative sum of days (black and coloured dotted lines) against the daily snowfall rate in mm w.e. per day. The red dashed lines guide the reading of the plot to get the snowfall rate and percentage of days responsible for 50% of the total snowfalls. Note the linear x-axis between 0 and 0.05 mm w.e. day^{-1} and logarithmic above.

Over the whole 5-year period, the precipitation amounts in the observations, ERA5 and ECHAM6-wiso have a comparable seasonal amplitude: from 0.03 to 0.1 mm w.e. day^{-1} for the observations (black in Fig. 5a), from 0.04 to 0.11 mm w.e. day^{-1} for ERA5 (blue in Fig. 5a) and from 0.04 to 0.1 mm w.e. day^{-1} for ECHAM6-wiso (light green in Fig. 5a). The three precipitation timeseries show a very similar seasonality, with an increase in snowfall rate at the end of the summertime (from

January to February) and in the middle of the winter (from June to July), as well as a decrease from July to December (Fig. 5a).

All three precipitation cumulative sums given by the observations, ERA5 and ECHAM6-wiso show a similar shape with a faster increase with increasing snowfall rates (plain lines in Fig. 5b). The cumulative sums from ERA5 and ECHAM6-wiso

430   are superposed in the whole range of snowfall rates, whereas the precipitation cumulative sum is lower for the observations up to 0.35 mm w.e. day^{-1}, where the three curves meet.

In the observations, 50% of the total snowfalls over five years is due to precipitation events with a snowfall rate above 0.32 mm w.e. day^{-1} (red dashed lines and black plain line in Fig. 5b), which represent only 6% of all days within the 5-year period (red dashed lines and black dotted line in Fig. 5b). It should be noted that these results are dependent on the precipitation

435   samples collected on site, which have biases (i.e. too little precipitation to collect or blown snow instead of true precipitation, Sect. 2.3). Similarly, in ERA5 precipitation, 50% of the total snowfalls is due to precipitation events with snowfall rates above 0.27 mm w.e. day^{-1} which corresponds to 7% of all days (Fig. 5b). In ECHAM6-wiso simulations, 50% of the total snowfalls is due to precipitation events with snowfall rates above 0.28 mm w.e. day^{-1} which corresponds to 6% of all days (Fig. 5b).

440   For all three timeseries (observations, ERA5 and ECHAM6-wiso), we find that the largest precipitation events described above (contributing to 50% of the total accumulation) occur alongside higher temperatures than average. In the observations, the mean temperature during all precipitation days within the 5-year period and with snowfall rates above 0.32 mm w.e. per day is 2.8°C warmer than the mean temperature over the whole period (-52.1°C). For ERA5, the mean temperature (given by ERA5) during the largest precipitation events with snowfall rates above 0.27 mm w.e. per day is 7.7°C above the mean

445   temperature of -49.5°C. Lastly, for ECHAM6-wiso, the mean temperature (given by the model) during the largest precipitation events with snowfall rates above 0.28 mm w.e. per day is 5.7°C above the mean temperature of -51.1°C. These results are in agreement with previous studies (Kino et al., 2021; Servettaz et al., 2023).

3.3.2 Precipitation isotopic composition

The daily temporal variability of the precipitation isotopic composition ($\delta^{18}O$ and d-excess) from both observations and

450   ECHAM6-wiso simulations is presented in Fig. 6, together with the corresponding mean annual cycles over the same period. In this section, all mean values across the whole period are given with an uncertainty corresponding to the SEM (see Sect. 3.2.1).

The observed precipitation $\delta^{18}O$ shows a large seasonal cycle, ranging from -82.6‰ to -21.8‰, with higher values in the summertime and lower values in the wintertime (dark blue dots in Fig. 6a), following the atmospheric temperature (grey line

455   in Fig. 6a). The mean value over the whole period is -56.2 ± 0.5‰ (dark blue dot in Fig. 6b). In comparison, the daily precipitation $\delta^{18}O$ modelled by ECHAM6-wiso show a similar seasonality as the observations, with higher and lower $\delta^{18}O$ in the summertime and wintertime respectively, and a comparable amplitude with values ranging from -82.9‰ to -22.8‰ (blue triangles in Fig. 6a). However, the mean modelled $\delta^{18}O$ in precipitation over the whole period is higher than the observed

one (-52.7 ± 0.5‰, blue triangle in Fig. 6b). The precipitation-weighted overall means are higher than the arithmetic means,

460 for both observations and ECHAM6-wiso simulations (-53.4 ± 0.5‰ and -45.7 ± 0.5‰, respectively, dark blue dot and blue

triangle in Fig. 6c).

The observed mean annual cycle (arithmetic monthly means) in the precipitation δ¹⁸O is characterised by the highest δ¹⁸O in

December (-46.5‰) and the lowest δ¹⁸O in June (-62.0‰, dark blue dots in Fig. 6b). In comparison, the modelled mean

annual cycle shows a similar seasonality but systematically higher than the observed one, ranging from -59.9‰ in June to -

465 38.4‰ in December (blue triangles in Fig. 6b). The difference between the observations and ECHAM6-wiso results is

especially large in the summertime (November to January), with a maximum difference of 8.1‰ in December.

The observed and modelled precipitation-weighted δ¹⁸O mean annual cycles also show a similar seasonality (Fig. 6c).

However, the bias between ECHAM6-wiso and observations is visible throughout the whole year, with a maximum

difference of 10.2‰ in October (Fig. 6c). The large difference between the observations and ECHAM6-wiso during the

470 summertime (arithmetic mean, Fig. 6b) decreases when the precipitation δ¹⁸O is weighted by the precipitation amounts (Fig.

6c).
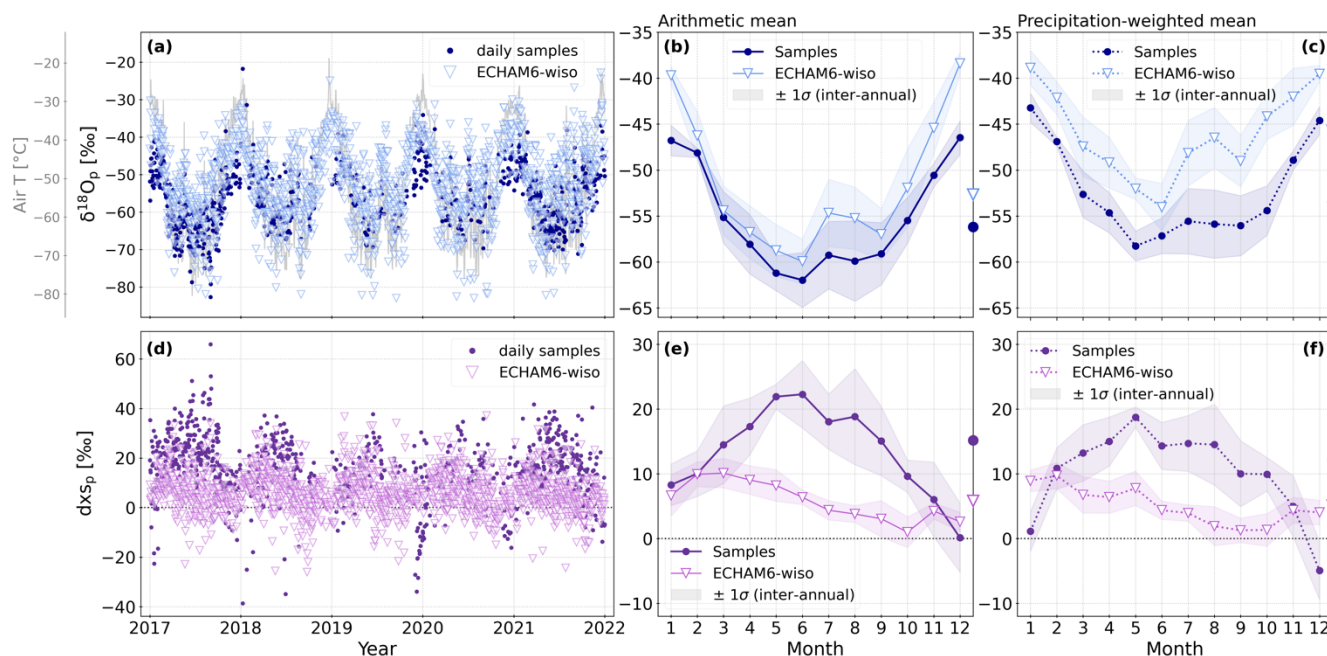
Figure 6. Observed and modelled precipitation isotopic composition at Dome C. Panels (a) and (d) show the 5-year time series (2017-
2021) for δ¹⁸O and d-excess (dxs) respectively. The dots represent the daily samples collected in the field (sample description in Sect. 2.3)
475 and the triangles represent the daily precipitation isotopic composition modelled by ECHAM6-wiso (description of simulations in Sect.
2.5). In grey in panel (a) is displayed the atmospheric temperature measured at 3 m (described in Sect. 2.4.1). Panels (b) and (e) show the
observed (dots) and modelled by ECHAM6-wiso (triangles) mean annual cycle, calculated over the period 2017-2021 (arithmetic means)
for δ¹⁸O and d-excess, respectively. The shaded area represents the inter-annual variability around the mean annual cycle (one standard
deviation). The markers on the right vertical axis indicate the mean observed and simulated precipitation isotopic composition over the
480 whole period. Panels (c) and (f) are the same as (b) and (e) but showing the weighted monthly means (by precipitation amounts).

The d-excess in the precipitation samples also shows a large seasonal amplitude, with values ranging from -38.6‰ to 65.9‰ (dark purple dots in Fig. 6d). d-excess is in anti-phase to δ^{18}O, with maximum values found in the wintertime and minimum values in the summertime, which have been previously identified by Stenni et al. (2016) and Dreossi et al. (2023). The mean observed precipitation d-excess over the whole period is equal to 15.2 ± 0.5‰ (dark purple dot in Fig. 6e). In comparison, the daily precipitation d-excess modelled by ECHAM6-wiso has a lower amplitude with values ranging from -26.0‰ to 37.2‰ (violet triangles in Fig. 6d). The overall mean modelled d-excess is also lower than the observations with a value of 5.8 ± 0.3‰ (violet triangle in Fig. 6e). The precipitation-weighted overall means are lower than the arithmetic means, for both observations and ECHAM6-wiso results (12.2 ± 0.5‰ and 5.1 ± 0.3‰, respectively, dark purple dot and violet triangle in Fig. 6f).

The observed mean annual cycle (arithmetic monthly means) in the precipitation d-excess is characterised by the lowest value in December (0.1‰) and the highest value in June (22.3‰, dark purple dots in Fig. 6e). In comparison, the mean annual cycle in the modelled precipitation d-excess has a lower amplitude than the observed one and a different timing in the minimum and maximum (from 1.0‰ in October to 10.1‰ in March, violet triangles in Fig. 6e). As opposed to δ^{18}O, the difference between the observations and ECHAM6-wiso simulations is large in the wintertime (April to October), with a maximum difference of 15.9‰ in June.

Compared to the arithmetic mean annual cycles for d-excess, the bias between the precipitation-weighted monthly means in ECHAM6-wiso and the observations is reduced in the winter but increased in the summer months January and December (Fig. 6f). The maximum difference is also lowered to 12.6‰ and found later in the year (August, Fig. 6f).

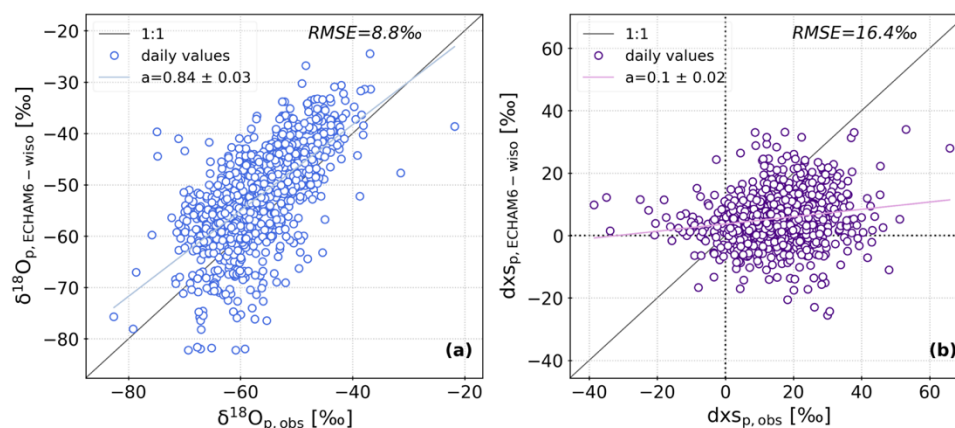**Figure 7.** Daily observed precipitation δ^{18}O (a) and d-excess (b) versus daily modelled precipitation isotopic composition at Dome C. All precipitation samples collected between 2017 and 2021 are shown (described in Sect. 2.3), together with the corresponding daily values from ECHAM6-wiso simulation results (described in Sect. 2.5). The coloured lines correspond to the linear fits between the observations and the model results (slope coefficients given in legends, both linear regression coefficients are significant with a p-value < 0.001).

We evaluate the performance of ECHAM6-wiso to model the observed daily precipitation isotopic composition in Fig. 7. The daily precipitation δ^{18}O modelled by ECHAM6-wiso shows a good agreement with the observations, with a linear

regression slope of 0.84 ± 0.03 (1.0 being the perfect fit) and a root mean square error (RMSE) of 8.8‰ (Fig. 7a). The model

510   mostly overestimates the observations with an increase in bias towards more depleted values (Fig. 7a). For d-excess, the

ECHAM6-wiso model results only poorly represent the observations, with a linear regression slope of 0.1 ± 0.02 and a

RMSE of 16.4‰ (Fig. 7b). These results are similar to the comparison of the precipitation samples and ECHAM6-wiso

simulation results between 2008 and 2017 (RMSE=6.1‰ for δ^{18}O and 13.6‰ for d-excess, Dreossi et al., 2023).

3.3.3 Isotope versus temperature relationships in precipitation

515   From the isotopic composition of the daily precipitation samples collected on site and the corresponding daily average

temperature measured at 3 m above the surface (described in Sect. 2.4.1), we determine the following linear relationships

over the 2017-2021 time-period:

$$\delta^{18}O_p = 0.47 \pm 0.01 \times T_{3m} - 31.2 \pm 0.6 ‰ \tag{1}$$

$$\delta D_p = 3.3 \pm 0.1 \times T_{3m} - 262 \pm 4 ‰ \tag{2}$$

520   Equation (1) has a coefficient of determination (R^2) of 0.62 and Eq. (2) has a R^2 of 0.63. Both linear regression slopes are

significant (p-values < 0.001, Fig. A1). There are no significant changes in the linear relationships if using the daily mean

atmospheric temperature of the day before the sample collection day instead of the daily mean temperature of the sampling

day itself (Fig. A1). The slopes in Eq. (1) and (2) are also comparable to the ones found for the 2008-2010 period (0.49 ±

0.02 for δ^{18}O, Stenni et al., 2016) and for the 2008-2017 period (0.52 ± 0.01 for δ^{18}O, 3.52 ± 0.07 for δD, Dreossi et al.,

525   2023).

In ECHAM6-wiso simulations, the linear relationships between the modelled precipitation isotopic composition and the

modelled temperature differ from the observed ones:

$$\delta^{18}O_{p, ECHAM6wiso} = 0.68 \pm 0.02 \times T_{2m, ECHAM6wiso} - 17.0 \pm 0.9 ‰ \tag{3}$$

$$\delta D_{p, ECHAM6wiso} = 5.3 \pm 0.1 \times T_{2m, ECHAM6wiso} - 134 \pm 6 ‰ \tag{4}$$

530   These relationships are also established over the period from 2017 to 2021. Equation (3) has a R^2 of 0.54 and Eq. (4) has a R^2

of 0.57. Both linear regression slopes are significant (p-values < 0.001, Fig. A2).

4 Discussion

4.1 Contribution of precipitation to the snow isotopic composition

In this section we discuss the contribution of the precipitation isotopic composition to the intra-monthly and seasonal

535   variability in the snow δ^{18}O and d-excess at Dome C, by comparing the observations and the results from the SISG

experiments (described in Sect. 2.5).

4.1.1 Surface snow

Some of the features observed in the surface snow $\delta^{18}O$ variability are reproduced by the different experiments performed with the SISG model (Fig. 8a). For example, the observed summer $\delta^{18}O$ values in the surface snow are correctly reproduced

540   in four out of five experiments ("iso from T & cst accu", "iso from T & ERA5 accu", "iso from wg. mm & obs accu", "iso from ar. mm & obs accu"). All five experiments correctly reproduce the seasonality in $\delta^{18}O$ observed in the surface snow, with higher values in the summer and lower values in the winter (Fig. 8a and b). In addition, the two model experiments "iso from T & ERA5 accu" and "iso from ECHAM6 & ECHAM6 accu" reproduce some of the short-term increases in the surface snow $\delta^{18}O$ during the wintertime, such as the events in August 2018, July 2020, or August 2021 (orange shadings in

545   Fig. 8a). The other three experiments fail to reproduce these events because of the inputs given to the SISG model: either a constant daily precipitation that weighs equally the days with high or low $\delta^{18}O$ ("iso from T & cst accu") or a daily isotopic composition that does not vary within one month and fails to represent the high $\delta^{18}O$ events ("iso from wg. mm & obs accu" and "iso from ar. mm & obs accu", Fig S2 in Supplement S3.1).
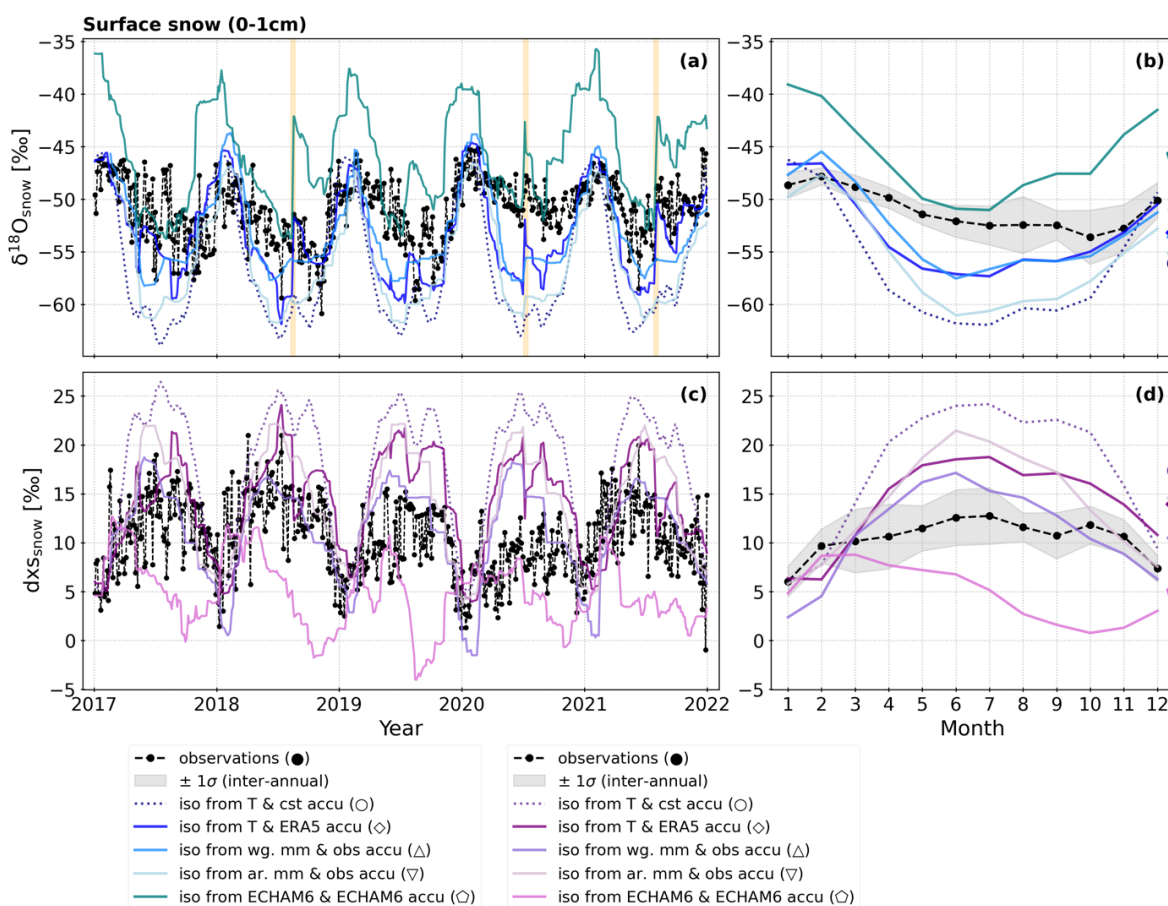
550   **Figure 8.** Comparison between observed and simulated surface snow (0 to 1 cm depth) isotopic composition at Dome C. Panels (a) and (c) show the 5-year time series (2017-2021) of $\delta^{18}O$ and d-excess (dxs) respectively. The black dots represent the horizontal average between

the two samples taken at the two locations 50 m apart on the sampling lines (described in Sect. 2.2, also presented in Fig. 3). The coloured lines (dotted and plain) represent the different SISG model experiments (described in Table 3). In panel (a), the orange vertical shadings highlight three specific events (August 2018, July 2020, August 2021). Panels (b) and (d) show the mean annual cycles (monthly means) of $\delta^{18}O$ and d-excess, respectively, calculated over the period 2017-2021. The black dots and line represent the observations and the shaded area represents the inter-annual variability around the mean annual cycle (one standard deviation). The coloured lines (dotted and plain) represent the different SISG experiments (described in Table 3). The markers on the right vertical axis indicate the mean isotopic composition of the observed and simulated snow surface over 5 years (see Table S2 in Supplement S3.2).

555

560   However, regardless of the model experiment, the amplitude of the seasonal cycle in the surface snow $\delta^{18}O$ is systematically overestimated compared to the observations (Fig. 8a and b). All five experiments fail to reproduce the slow decrease in $\delta^{18}O$ during the wintertime observed in the surface snow. This is particularly visible for the winters 2019 and 2020 where all simulated surface snow has too low $\delta^{18}O$ values (Fig. 8a). Most of the short-term variations in the snow $\delta^{18}O$ occurring within the month are also not reproduced by any of the experiments (Fig. 8a). In addition, the experiment "iso from

565   ECHAM6 & ECHAM6 accu" gives too high $\delta^{18}O$ compared to the observations throughout the whole time-period (blue-green lines in Fig. 8a and b), which is consistent with the positive bias between the precipitation-weighted $\delta^{18}O$ modelled by ECHAM6-wiso and the observations, identified in Sect. 3.3.2 (Fig. 6c).

As for $\delta^{18}O$, all model experiments fail to reproduce the variability in d-excess observed in the surface snow. Although in some of the experiments ("iso from T & cst accu", "iso from T & ERA5 accu", "iso from wg. mm & obs accu", "iso from ar.

570   mm & obs accu"), the low summer d-excess in the surface snow is well captured (Fig. 8c), all the simulated mean annual cycles have a too large amplitude (Fig. 8d). The experiment "iso from ECHAM6 & ECHAM6 accu" provides worse results than the other experiments (pink line in Fig. 8c and d), which can be explained by the poor representation of the observed precipitation-weighted annual cycle in d-excess by ECHAM6-wiso simulations, identified in Sect. 3.3.2 (Fig. 6f).

575   To evaluate which SISG experiment best represent the observed snow surface isotopic composition, we perform a linear regression between all modelled and observed monthly means $\delta^{18}O$ and d-excess in the five-year period. The linear regression slopes (a) and the RMSE between the model results and the observations are summarized in Table 4.

The best representation of the observed $\delta^{18}O$ in the surface snow is given by the experiment "iso from wg. mm & obs accu" (a=1.1, RMSE=3.4‰, Table 4). The experiment "iso from T & cst accu" results in the highest RMSE of all configurations

580   tested (RMSE=6.9‰, Table 4), which is expected due to the intermittent nature of precipitation at Dome C. In addition, the experiment "iso from ECHAM6 & ECHAM6 accu" gives a high RMSE (6.3‰, Table 4).

For d-excess, out of the five model experiments, "iso from wg. mm & obs accu" gives the lowest RMSE (3.9‰, Table 4). As for $\delta^{18}O$, the experiment "iso from T & cst accu" results in the highest RMSE (8.8‰, Table 4). Lastly, the experiment "iso from ECHAM6 & ECHAM6 accu" has a RMSE of 7.1‰ and a non-significant slope compared to the observations (p-value

585   > 0.05).

Table 4. Linear regression slope (a) and RMSE between the observed and modelled monthly mean isotopic composition of the surface layer ($\delta^{18}O$ in normal font, d-excess in parenthesis and italic). The sample size is 60 for all experiments except "iso from wg. mm & obs

accu" and "iso from ar. mm & obs accu" (n=59). All linear slopes are significant (p-value < 0.05), except the ones marked with an asterisk
590 (*, p-value > 0.05).

Experiment	"Iso from T & cst accu"	"Iso from T & ERA5 accu"	"Iso from wg. mm & obs accu"	"Iso from ar. mm & obs accu"	"Iso from ECHAM6 & ECHAM6 accu"
a	1.4 *(1.4)*	1.2 *(0.9)*	1.1 *(0.9)*	1.3 *(1.1)*	1.1 *(0*)*
RMSE (‰)	6.9 *(8.8)*	3.7 *(5.3)*	3.4 *(3.9)*	5.8 *(5.5)*	6.3 *(7.1)*

4.1.2 Subsurface snow

For $\delta^{18}O$ in the subsurface snow, we find comparable results as for the surface layer. We find that all five model experiments
fail to capture the short-term variations in the subsurface snow, and all experiments result in a too-large amplitude in the
595 mean annual cycle over five years (Fig. 9a and b). The systematic positive bias given by the model experiment "iso from
ECHAM6 & ECHAM6 accu" is also visible in the simulated subsurface layer (Fig. 9a and b). In addition, all five model
experiments provide a mean annual cycle shifted compared to the observed one, with a maximum $\delta^{18}O$ occurring one to two
months later than the observed maximum (Fig. 9b).
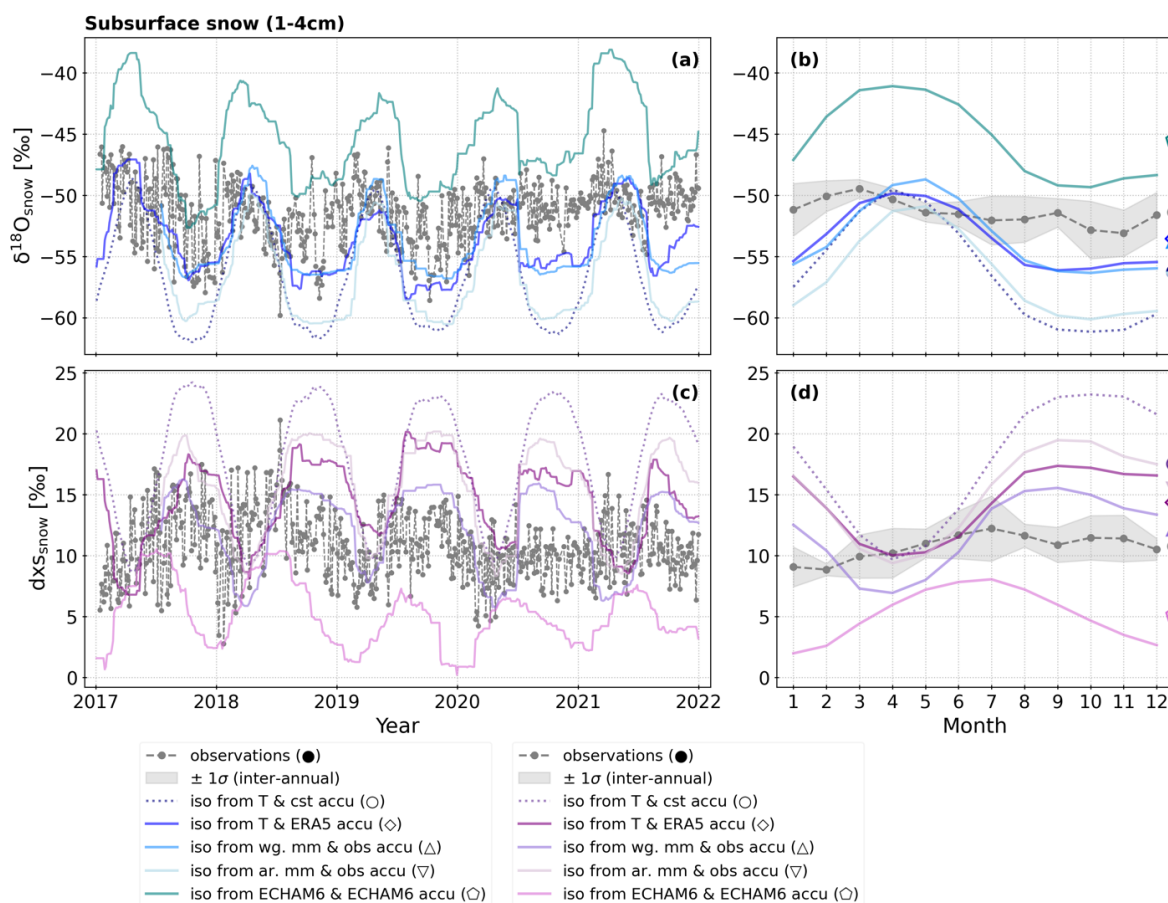
Figure 9. Comparison between observed and simulated subsurface snow (1 to 4 cm depth) isotopic composition at Dome C. Panels (a) and
600 (c) show the 5-year time series (2017-2021) of $\delta^{18}O$ and d-excess (dxs) respectively. The grey dots represent the horizontal average

22

between the two samples taken at the two locations 50 m apart on the sampling lines (described in Sect. 2.2, also presented in Fig. 3). The coloured lines (dotted and plain) represent the different SISG model experiments (described in Table 3). Panels (b) and (d) show the mean annual cycles (monthly means) of $\delta^{18}O$ and d-excess, respectively, calculated over the period 2017-2021. The grey dots and line represent
605 the observations and the shaded area represents the inter-annual variability around the mean annual cycle (one standard deviation). The coloured lines (dotted and plain) represent the different SISG experiments (described in Table 3). The markers on the right vertical axis indicate the mean isotopic composition of the observed and simulated snow subsurface over 5 years (see Table S2 in Supplement S3.2).

For d-excess, we find that four out of five of the model experiments ("iso from T & cst accu", "iso from T & ERA5 accu",
610 "iso from wg. mm & obs accu", "iso from ar. mean & obs accu") give too high d-excess variations over time, which is reflected in the too large amplitude of the modelled mean annual cycle compared to the observed one (Fig. 9c and d). As for $\delta^{18}O$, the annual cycle in d-excess modelled in these three experiments is shifted, with the minimum in d-excess found two months later than the observed one (Fig. 9d).

On the other hand, although giving too low d-excess compared to the observations, the experiment "iso from ECHAM6 &
615 ECHAM6 accu" results in a similar mean annual cycle as in the observations, with minimum d-excess in the summertime and maximum d-excess during the wintertime (pink line in Fig. 9d). However, because the precipitation d-excess modelled by ECHAM6-wiso poorly represent the observations (Fig. 6e and f), we argue that the good resemblance (besides the negative bias) between the modelled and observed d-excess in the subsurface snow is due to compensating effects between the precipitation d-excess and precipitation amounts.

620

As for the surface snow, we perform a linear regression between all modelled and observed monthly means $\delta^{18}O$ and d-excess. The linear slopes (a) and the RMSE between the model results and the observations are summarized in Table 5.

Contrary to the surface layer, the best representation of $\delta^{18}O$ in the subsurface layer is given by the experiment "iso from T & ERA5 accu" (a=0.8, RMSE=3.2‰, Table 5). The model experiment "iso from ECHAM6 & ECHAM6 accu" gives the
625 best correlation with observations, although with the highest RMSE (a=1.1, RMSE=6.7‰, Table 5).

For d-excess in the subsurface snow, only the experiment "iso from ECHAM6 & ECHAM6 accu" gives a significant slope with the observations (a=0.8, RMSE=6.0‰, Table 5) while all other experiments have a non-significant linear slope with the observations (p-value > 0.05, Table 5). However, as stated above, we argue that this good agreement between the simulated subsurface snow in the experiment "iso from ECHAM6 & ECHAM6 accu" is due to compensating effects between the
630 precipitation d-excess and precipitation amounts.

Table 5. Linear regression slope (a) and RMSE between the observed and modelled monthly mean isotopic composition of the subsurface layer ($\delta^{18}O$ in normal font, d-excess in parenthesis and italic). The sample size is 60 for all experiments except "iso from wg. mm & obs accu" and "iso from ar. mm & obs accu" (n=54). All linear slopes are significant (p-value < 0.05), except the ones marked with an asterisk
635 (*, p-value > 0.05).

Experiment	"Iso from T & cst accu"	"Iso from T & ERA5 accu"	"Iso from wg. mm & obs accu"	"Iso from ar. mm & obs accu"	"Iso from ECHAM6 & ECHAM6 accu"
a	1.0 *(0.5*)*	0.8 *(0.2*)*	0.5 *(0.4*)*	0.7 *(0.3*)*	1.1 *(0.8)*
RMSE (‰)	6.2 *(8.4)*	3.2 *(5.1)*	3.5 *(3.5)*	6.1 *(6.0)*	6.7 *(6.0)*

23

4.1.3 SISG setup and inputs

In the Sect. 4.1.1 and 4.1.2, we showed that none of the five SISG experiments fully represent the variability observed in the snow surface and subsurface isotopic composition (δ^{18}O and d-excess). However, the model was designed with a fixed depth for both snow samples to best represent the observations, although the depths of the samples collected in the field might have varied over time (Sect. 2.2). Changing the sample depths in the SISG model does not significantly improve the agreement between the model results and the observations (Table S3 in Supplement S3.3).

The inputs of the model might also explain some of the discrepancies between the observed and modelled snow layers. For example, there are fewer small precipitation events in the observations than given by ERA5 and ECHAM6-wiso (Fig. 5b), which could lead to an underestimation of the contribution of smaller precipitation events (e.g. diamond dust) to the total accumulation and explain the differences between the experiments "iso from wg. mm and obs accu" and "iso from ar. mm and obs accu" and the observations (Fig. 8 and 9). Some snowfall events in ERA5 and ECHAM6-wiso could also be occurring too early or too late and explain why the short-term increases and decreases in the snow isotopic composition are not reproduced in the experiments using ERA5 and ECHAM6-wiso precipitation amounts (Fig. 8a and c, Fig. 9a and c). In addition, we scaled up all three precipitation timeseries to match the mean annual accumulation of 8 cm year^{-1} at Dome C (Sect. 2.5), although this value can vary and estimations over other time periods have given higher mean accumulation rates (e.g. Frezzotti et al., 2005). Lastly, in three out of five experiments, we used an artificial daily precipitation isotopic composition (Sect. 2.5), but none of these represent accurately the observed precipitation isotopic composition (Fig. S2 in Supplement S3.1).

4.2 Transfer of the isotopic signal between precipitation, surface, and subsurface snow

In this section we discuss the potential processes at the surface of the ice sheet responsible for the discrepancies between the precipitation signal and the observed snow surface and subsurface layers and assess the overall impact of these processes on the transfer of the isotopic signal between precipitation to the snow.

4.2.1 Short-term, inter-annual and seasonal variability in the snow isotopic composition

Several studies have shown that water vapor fluxes between the lower atmosphere and the snow can modify the isotopic composition of the snow surface (Casado et al., 2021b; Hughes et al., 2021; Wahl et al., 2021, 2022) and deeper firn cores (Dietrich et al., 2023). Although the impact depends on the isotopic composition of the atmospheric water vapor above, sublimation generally leads to an enrichment in δ^{18}O of the snow surface and a lowering of its d-excess. In addition, Casado et al. (2018) hypothesized that the inter-annual variability of the summer snow surface isotopic composition is related to the strength of metamorphism and surface vapor fluxes.

We showed that at Dome C, sublimation occurs during the summertime (Fig. 2a) and that there is a net annual sublimation of snow (Fig. 2b), which means that the surface snow isotopic composition must have been affected by these fluxes. In the

24

snow samples collected at the surface and just below, we observe some inter-annual variability in the vertical difference between the surface and subsurface snow isotopic compositions (Fig. 4). This difference between the layer exposed to the atmosphere and the subsurface could be explained by the inter-annual variability in vapor fluxes (Fig. 2a). For example, the snow surface is most enriched in δ^{18}O compared to the subsurface in December 2019 and January-February 2020 (Fig. 4). In parallel, we observe strong sublimation occurring in November and December 2019 (Fig. 2a), probably enriching the snow surface in δ^{18}O, and leading to a much more enriched surface snow compared to the subsurface in the samples collected in the following months. Yet, the highest sublimation rate occurring in December 2018 (Fig. 2a) is not necessarily reflected in the vertical difference between the surface and subsurface snow layers (Fig. 4). This could be explained by the length of the sublimation period, critical for the overall impact on the snow surface (Hughes et al., 2021; Wahl et al., 2022).

The mean seasonal cycle in the difference between the surface and subsurface isotopic compositions can, on the other hand, most likely be explained by the depths of the samples that integrate the precipitation events fallen during the last couple of months for the surface sample and up to the previous winter for the subsurface sample (assuming no removal or redistribution and no compaction of snow, Fig. S3 in Supplement S3.4). The higher δ^{18}O and lower d-excess in the summer precipitation compared to the winter precipitation (Fig. 6) explains why the mean summer surface snow is enriched in δ^{18}O and has a lower d-excess than the subsurface snow (Fig. 4).

If we would include vapor fluxes in the simple SISG model, the amplitude of the modelled seasonal cycle in the surface snow would be increased (summer months enriched in δ^{18}O and reduced in d-excess), increasing the discrepancy with the observations (Fig. 8b and d). This shows that an additional process reducing the amplitude of the mean annual cycle in the snow surface takes place. Diffusion is a good candidate.

The isotopic composition of the snowpack is affected by diffusion of water molecules along isotopic and temperature gradients (Johnsen et al., 2000; Gkinis et al., 2014). The addition of this process in our model would possibly reduce the too large amplitude of the seasonal cycles in the synthetic snow layers to match the observations (Fig. 8b and, 9b and d). In addition, some of the short-term variations observed in the subsurface snow that are not explained by the incoming precipitation (Fig. 9a and c) could instead be explained by changes occurring in the surface snow and diffused downwards, as suggested by Casado et al., (2018).

Lastly, although Dome C is not affected by strong katabatic winds, surface winds can still be strong enough to erode and redistribute the snow (Libois et al., 2014). In a study of the process of snow accumulation at Dome C, Picard et al. (2019) showed that the surface snow changes very frequently due to snow erosion and accumulation by small patches (10% of the surface only is affected by each precipitation events), and that the snow in a patch can be as old as one year at the surface, while another patch was deposited by the last precipitation event. In the snow samples collected at Dome C, we observe higher differences in δ^{18}O and d-excess between two consecutive sampling days of the surface and subsurface snow when the wind speed increases from one sampling day to another (Fig. S4 in Supplement S4), as well as a decrease in δ^{18}O and d-excess vertical difference between the surface and the subsurface snow (Fig. S5 in Supplement S4). This could indicate that

some of the short-term variations observed in the snow surface isotopic composition that cannot be explained by new precipitation falling on the surface (Fig. 3, 8a and c) be caused instead by wind erosion and redistribution.

The wind blowing at the surface of the ice sheet during or beside snowfall could lead to a mixing of new precipitation with already deposited snow. This process was proposed by Casado et al. (2018) to explain the slow decrease in the surface snow
705 $\delta^{18}O$ during the winter, a pattern observed in our study (Fig. 3a and b) and that cannot be explained by precipitation only (Fig. 8a and b).

Overall, our results show evidence that the snow isotopic composition is affected by post-depositional processes at different timescales. Disentangling the contribution of the different processes described above on the final isotopic signal found in the snow is beyond the scope of this study and requires the use of an isotope-equipped snowpack model that includes post-
710 depositional processes at the surface, such as the one developed recently by Wahl et al. (2022) and Dietrich et al. (2023).

4.2.2 Mean effect of post-depositional processes

The datasets presented in this study permit to quantify the overall impact of post-depositional processes on the snow isotopic composition. Table 6 summarizes the mean isotopic composition over five years of the precipitation (weighted average by the observed precipitation amounts, see Sect. 2.5.1), the snow surface, and the subsurface snow. The mean isotopic
715 composition of precipitation excluding all samples with negative d-excess and modelled by ECHAM6-wiso are also provided. All mean values are given with their respective standard error (see Sect. 3.2.1 and Supplement S2) and 95% confidence interval (Student t-test, Supplement S2).

Table 6. Five-year mean isotopic composition of precipitation (weighted by the observed precipitation amounts) and snow samples ($\delta^{18}O$
720 in normal font, d-excess in parenthesis and italic). The mean values are given with their respective standard error (see Sect. 3.2.1) and in brackets their 95% confidence interval (Student t-test, Supplement S2).

	Observations	Observations (excl. samples with dxs < 0)	ECHAM6-wiso
Precipitation-weighted (‰)	-53.4 ± 0.5 [1.0] *(12.2 ± 0.5 [1.0])*	-54.3 ± 0.4 [0.9] *(13.9 ± 0.4 [0.8])*	-45.7 ± 0.5 [0.9] *(5.1 ± 0.3 [0.5])*
Surface snow (‰)	-51.0 ± 0.2 [0.4] *(10.4 ± 0.2 [0.5])*	– –	– –
Subsurface snow (‰)	-51.4 ± 0.1 [0.3] *(10.8 ± 0.1 [0.3])*	– –	– –

We express the mean effect of post-depositional processes at Dome C as the difference between the 5-year mean observed
725 precipitation-weighted isotopic composition of precipitation and the 5-year mean isotopic composition of the surface snow. Considering all precipitation and snow samples, the surface snow $\delta^{18}O$ is 2.4‰ higher than in precipitation and the surface snow d-excess is 1.8‰ lower than in precipitation (Table 6). However, to exclude any imprint of sublimation on the precipitation isotopic composition, we re-compute the mean isotopic composition of precipitation discarding all the samples with a d-excess below zero, as in Steen-Larsen et al. (2011). Although the zero threshold might be arbitrary, it is supported
730 by laboratory and field studies that showed a decrease in d-excess during snow sublimation and metamorphism (Hughes et

al., 2021; Casado et al., 2021b; Harris Stuart et al., 2023). In addition, Stenni et al. (2016) and Dreossi et al. (2023) already stated that some of the samples collected in the summertime at Dome C might have been affected by sublimation and we observe in the precipitation dataset presented here that the samples with very negative d-excess were collected during the summertime (e.g. December 2019, Fig. 6d) when sublimation occurred (Fig. 2a). We therefore argue that removing all

735 precipitation samples with a d-excess below zero improves the representation of the true precipitation falling at Dome C. Now considering this new precipitation timeseries, the δ^{18}O in the surface snow is 3.3‰ higher than in precipitation and the d-excess in the surface snow is 3.5‰ lower than in precipitation (Table 6). Both differences are significant on a 95% confidence level (Table 6).

The weighted mean isotopic composition of precipitation is computed using the observed precipitation amounts, estimated

740 from the weights of the samples collected on site (Sect. 2.3 and 2.5.1). However, as discussed in Sect. 4.1.3, these amounts might not accurately represent the precipitation falling at Dome C. Using the precipitation amounts given by ERA5 instead, the weighted mean δ^{18}O of precipitation is -57.6‰ and 18.0‰ for d-excess, which leads to larger differences between the precipitation and the snow surface: δ^{18}O in the surface snow is 6.6‰ higher than in precipitation and d-excess in the surface snow is 7.6‰ lower than in precipitation.

745 The discrepancies between the precipitation and the surface snow show that the mean isotopic composition of precipitation is not preserved from snowfall to the surface snow. On average over a 5-year period at Dome C, post-depositional processes lead to an enrichment in δ^{18}O of the snow surface by 3.3‰ to 6.6‰ (depending on which precipitation amounts are considered) and a lowering of d-excess in the snow surface by 3.5‰ to 7.6‰ compared to the precipitation signal. It is still to be determined the individual contribution of the different post-depositional processes (discussed in Sect. 4.2.1) on the

750 isotopic difference observed between the precipitation and the snow surface.

In contrast to the isotopic difference between the precipitation and surface snow, there is no significant difference between the mean surface and subsurface snow isotopic compositions, for both δ^{18}O and d-excess (Table 6). This shows that despite a seasonality in the vertical difference between the two snow layers (discussed in Sect. 4.2.1), the mean isotopic composition of the surface snow layer is preserved in the top few centimetres of the snowpack.

755 From the sampling of a 2 m snow pit at Dome C, Touzeau et al. (2016) reported mean values (plus-minus standard error of the mean) of -51.1 ± 0.2‰ and 9.1 ± 0.2‰ for the δ^{18}O and d-excess profiles, respectively. As found in our study for the upper layers of the snow, the average isotopic composition of the snow pit is enriched in δ^{18}O and has a lower d-excess than the mean incoming precipitation isotope signal.

760 The weighted-mean isotopic composition of precipitation modelled by ECHAM6-wiso is 7.7‰ higher in δ^{18}O and 7.1‰ lower in d-excess than the observed precipitation (Table 6, Fig. 6c and f). These large differences result from the biases identified between the modelled and observed precipitation isotopic composition (Sect. 3.3.2, Fig. 6 and 7), and show the limitations of using ECHAM6-wiso simulations to interpret the isotopic composition of the snow at Dome C. A thorough investigation of the biases in ECHAM6-wiso is beyond the scope of this study, but might arise from different processes in

765   the model, such as the environmental conditions at the moisture source region, the moisture transport and pathway, the

supersaturation parametrization or the condensation height and temperature above Dome C.

4.2.3 Seasonal $\delta^{18}O$ versus temperature relationships in precipitation and snow

In precipitation, the $\delta^{18}O$-temperature relationship is determined between the $\delta^{18}O$ in the daily precipitation samples and the

corresponding daily atmospheric temperature (Sect. 3.3.3, Eq. (1)). For the surface and subsurface snow, we determine the

770   relationships between the $\delta^{18}O$ composition of each snow sample and the weighted-average temperature (by precipitation

amounts) over the entire period during which precipitation accumulated and formed the snow sample (Fig. A3). We use the

observed precipitation amounts to determine this averaging period (Fig. S3 in Supplement S3.4). Table 7 summarizes the

linear regression slopes (a) with their standard errors and the coefficient of determination (R^2).

775   **Table 7.** Summary of mean seasonal $\delta^{18}O$ versus temperature linear relationships in precipitation and snow samples between 2017 and
2021. The slopes (a) are given with their standard error and all three slopes are significant (p-value < 0.001).

	Precipitation	Snow surface	Snow subsurface
a (‰ °C^{-1})	0.47 ± 0.01	0.17 ± 0.01	0.12 ± 0.02
R^2	0.62	0.25	0.1

We find a mean seasonal $\delta^{18}O$-temperature slope in precipitation of 0.47 ± 0.01‰ °C^{-1}, in agreement with previous studies

780   for the same location for earlier years (Stenni et al., 2016; Dreossi et al., 2023). We find a mean seasonal slope of $0.17 \pm$

0.01‰ °C^{-1} in the surface snow (top 1 cm) and a mean seasonal slope of 0.12 ± 0.02‰ °C^{-1} in the subsurface snow (1 to 4

cm, Table 7). The surface snow slope coincides with the one found for the snow top 1-2 mm at Dome C (0.14 ± 0.03‰ °C^{-1},

Touzeau et al., 2016) but is lower than the ones found by Casado et al. (2018) for similar samples in earlier years (slopes

ranging from 0.22 to 0.49‰ °C^{-1}). This difference can be due to uncertainties on the precipitation amounts used to determine

785   the averaging period of temperature (i.e. some precipitation days with colder temperatures are not captured), the method used

to determine the averaging period of temperature (i.e. assumes that snowfall is not redistributed or removed and does not

include snow compaction, Supplement S3.4), or due to the different method used in Casado et al. (2018) where they compute

the slope as the ratio of the maximum amplitude in $\delta^{18}O$ and the maximum amplitude in temperature.

Our results indicate that deriving a temporal slope from seasonal variations of $\delta^{18}O$ in the surface snow to be used for ice

790   core studies is not consistent with other in-situ and proxy temperature reconstructions. First, the surface snow $\delta^{18}O$ is not

showing a symmetric seasonal cycle. Instead, the $\delta^{18}O$ minimum is shifted towards spring (Fig. 3, Sect. 3.2.1) while the

minimum temperature occurs in winter. Secondly, our determination of the seasonal relationship between the snow $\delta^{18}O$ and

the atmospheric temperature results in a weaker correlation and a lower slope (0.12 – 0.17‰ °C^{-1}, Table 7) than what is

found for precipitation (0.47‰ °C^{-1}, Table 7). Using the $\delta^{18}O$-temperature slope found in the upper layers of the snow for

795   temperature reconstructions from ice cores would lead to unrealistic glacial-interglacial temperature change exceeding 30°C.

The change in the seasonal $\delta^{18}O$-temperature relationship between the precipitation and the upper layers of the snow shows

the difficulty to interpret quantitatively the δ^{18}O variations in the snow at Dome C in terms of temperature. Instead, it provides the opportunity to document the effects of post-depositional processes at this site and improve the future quantitative interpretation of water isotopic records in ice cores from Dome C for longer timescales (decadal and longer

800 timescales).

4.3 Long-term perspectives for the interpretation of ice core isotope records

The classical paleothermometer approach (Lorius and Merlivat, 1975) to determine past temperature variations from the water isotopic profiles in ice cores uses the present-day spatial slope between the water isotopic composition of the surface snow and the local temperature. However, as illustrated in Casado et al. (2017), this spatial slope differs from the various

805 estimates of the temporal slope between temperature and δ^{18}O found in the literature and in this study, determined for different regions and timescales. These discrepancies show the need of calibration of the isotopic paleothermometer. Such calibration has been done using alternative methods at the glacial-interglacial scale (e.g. borehole thermometry and firn properties, Buizert et al., 2021), or using isotope-enabled GCMs to determine the relationship between temperature and water isotopes during past periods (e.g. Werner et al., 2018). However, in these models, the absence of explicit modelling of

810 how the water isotopic signal is archived in the snow and firn limits their use for paleo-reconstructions.

To progress towards an accurate quantitative interpretation of isotopes in ice cores, we recommend developing a *proxy system model* that can be coupled to isotope-enabled GCMs. Such a model has been developed recently by Wahl et al. (2022) and Dietrich et al. (2023) for Greenland and includes mechanical processes leading to the recording of isotopes at the ice sheet's surface and in ice cores. The datasets presented in our study can therefore be useful to calibrate and validate this kind

815 of *proxy system model* at intra-annual, seasonal, and inter-annual timescales at the deep drilling site of the EPICA Dome C ice core.

5 Conclusions

We have presented the compilation of new and existing datasets of the isotopic composition of precipitation, snow surface and subsurface together with meteorological parameters, reanalysis products, model outputs and a simple modelling

820 approach to investigate the origin of the stable water isotopic signal in the upper layers of the snowpack at Dome C, East Antarctica.

From in-situ meteorological observations, we have quantified the amount of water vapor fluxes between the snow and the lower atmosphere. Our results show that vapor fluxes contribute to the surface mass balance at Dome C with a net annual mass loss of snow from 3.1 to 3.7 mm w.e. year^{-1} between 2018 and 2020, which corresponds to 12 to 15% of the annual

825 surface mass balance. Sublimation is relatively strong in the summertime and there is small condensation in the wintertime.

From the comparison between the snow surface and subsurface isotopic compositions and a simple modelling approach, we show that the precipitation deposited onto the ice sheet cannot explain the variability observed in the snow isotopic

29

composition (δ^{18}O and d-excess) at seasonal to intra-monthly timescales, highlighting the existence of post-depositional processes affecting the snow isotopic composition.

830   We quantified the cumulative effect of post-depositional processes on the surface snow over five years by comparing the mean isotopic compositions of the precipitation and the snow layers. Our results show that post-depositional processes lead to an enrichment of the snow surface (top 1 cm) in δ^{18}O by 3.3‰ to 6.6‰ (depending on the precipitation amounts considered) and a lowering of the surface snow d-excess by 3.5‰ to 7.6‰. In addition, our results show that the mean isotopic composition of the subsurface snow (1 to 4 cm depth) is not significantly different than the surface snow, which

835   indicates that the mean isotopic composition of the surface snow layer is preserved in the top centimetres of the snowpack and that the processes altering the precipitation isotopic signal mainly take place in the top one centimetre of the snow.

   In both the observations, ERA5 reanalyses and ECHAM6-wiso simulation, we showed that 50% of the accumulation at Dome C over five years occurs during large but rare precipitation events associated with warmer temperatures than average, leading to a warm bias in the δ^{18}O record of precipitation compared to the mean annual temperature. We further find

840   different seasonal relationships between the atmospheric temperature and δ^{18}O in the precipitation and the snow, showing the difficulty to interpret the variations of δ^{18}O in the snow at Dome C.

   Overall, our results show that post-depositional processes at the ice sheet's surface have an impact on the isotopic signal (both δ^{18}O and d-excess) found in the upper layers of the snowpack at Dome C, East Antarctica. The datasets presented in our study open the possibility to calibrate and validate *proxy system models* including post-depositional processes that are

845   needed to quantitatively attribute the different mechanisms building up the isotopic signal in the surface snow and to accurately reconstruct the climatic information from the water stable isotope records in ice cores.
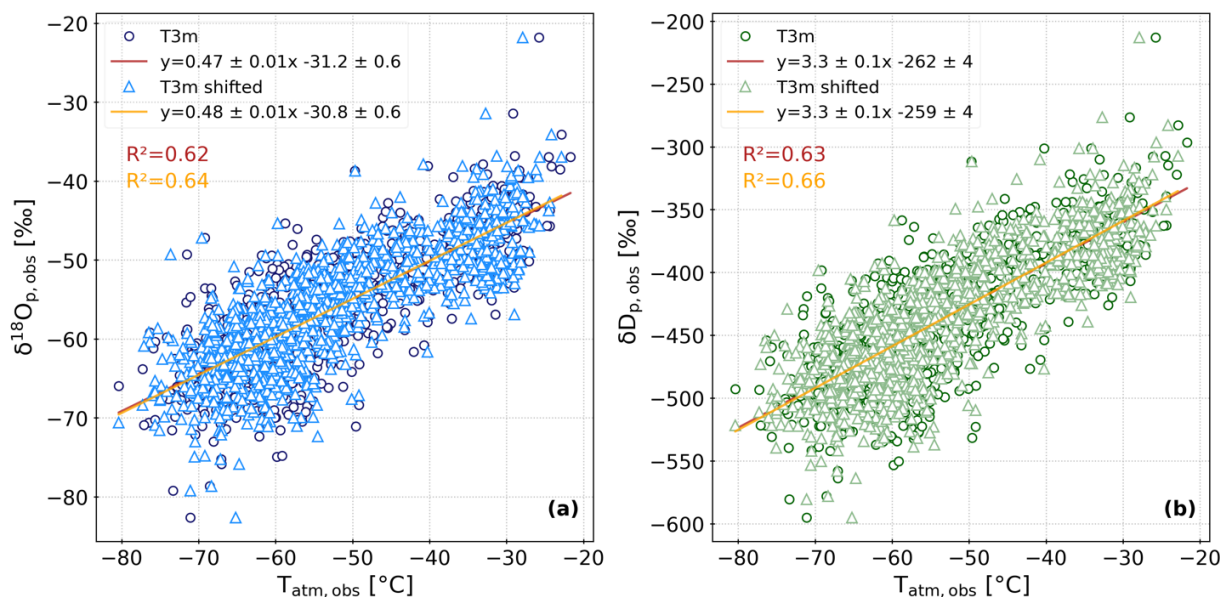
Figure A1. Daily observed precipitation δ^{18}O (a) and δD (b) versus observed daily mean temperature at Dome C. All precipitation samples collected between 2017 and 2021 are shown against the corresponding daily mean temperature (T3m, dark colours) and the daily mean temperature of the day before (T3m shifted, light colours). The linear regressions with the associated coefficients of determination (R^2) are
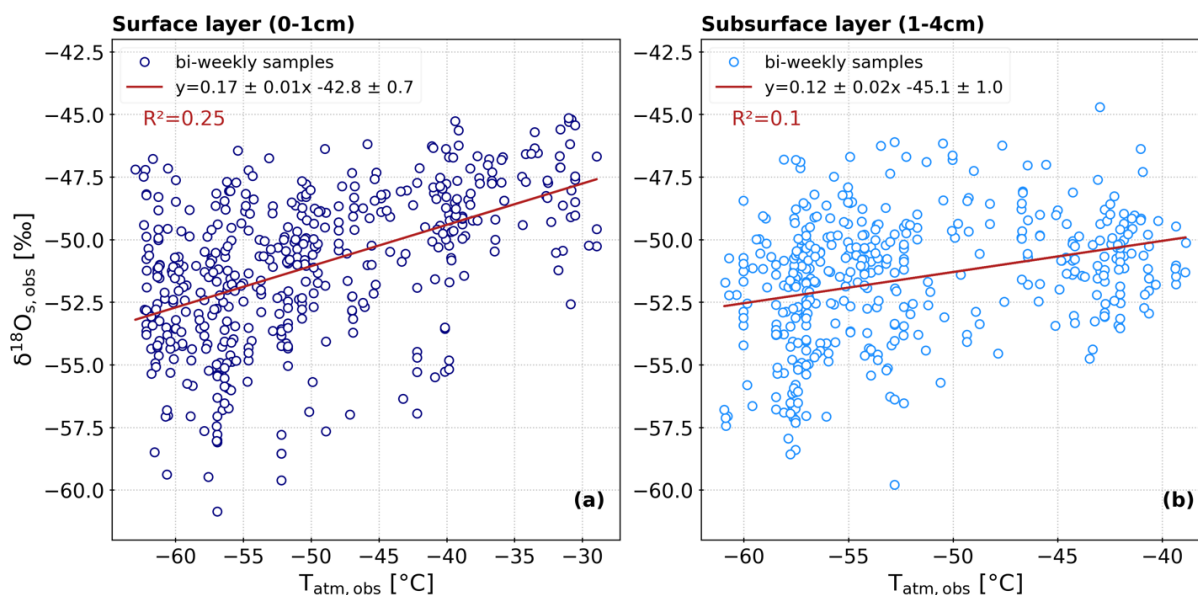
855   shown. Both linear slopes are significant (p-values < 0.001).
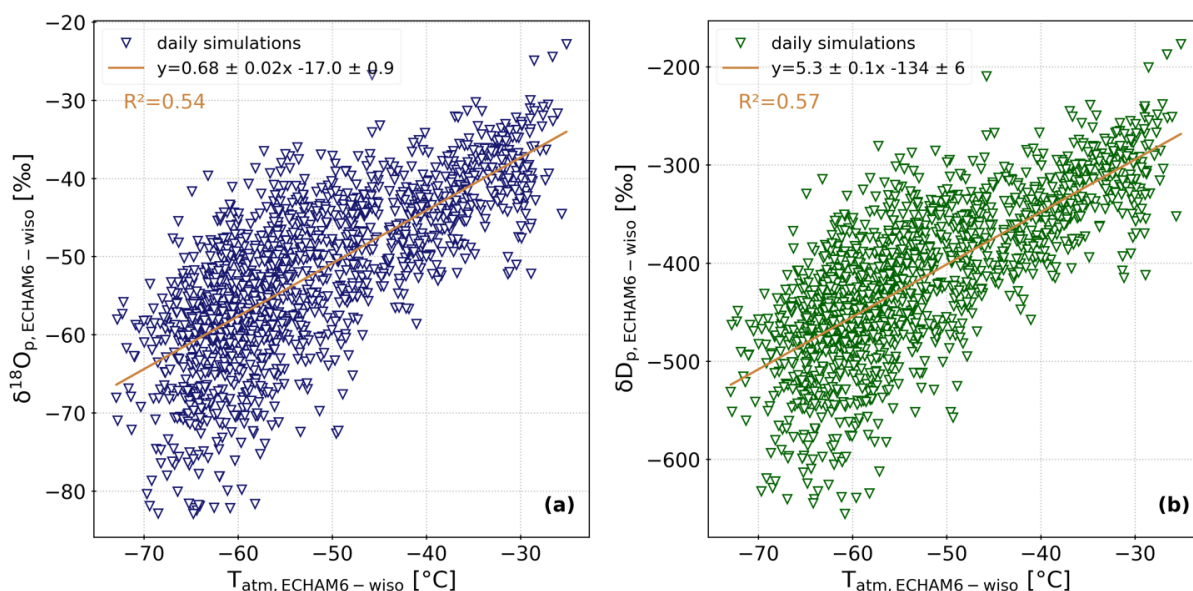
Figure A2. Daily precipitation δ^{18}O (a) and δD (b) modelled by ECHAM6-wiso versus daily mean temperature modelled by ECHAM6-wiso. The linear regressions with the associated coefficients of determination (R^2) are shown. Both linear slopes are significant (p-values <

860   0.001).

31

Figure A3. Bi-weekly observed snow surface (a) and subsurface (b) $\delta^{18}O$ versus temperature at Dome C. All snow samples collected between 2017 and 2021 are shown against the weighted-average temperature (by precipitation amounts) over the period corresponding to the accumulation of the snow samples (see Sect. 4.2.3). The linear regressions with the associated coefficients of determination (R^2) are shown. Both linear slopes are significant (p-values < 0.001).

Code availability. Python scripts for the estimations of moisture fluxes with the bulk method and for the SISG model will be uploaded on Zenodo upon acceptance of the article and DOIs will be provided.

Data availability. The DOIs for the two datasets in review with PANGAEA will be provided as soon as possible and latest at publication date. The CNR4 dataset will be published upon acceptance of the article.

Author contribution. IO, HCSL, BS and AL designed the study and contributed to the analysis. IO performed the formal analysis and visualization. HCSL, BS and AL supervised the study. MC designed the first version of the simple model (SISG) and provided inputs to the study. GP and LA acquired and shared radiation data (CNR4) and coordinated the snow sample collection executed by the winter-over staff. CG acquired meteorological data (USt) and provided inputs to the study. GD and IO performed the isotopic analysis of the precipitation samples. BM performed the isotopic analysis of the snow samples. AC and MW performed the ECHAM6-wiso simulation. IO wrote the first draft of the manuscript and all authors contributed to reviews and edits.

Competing interests. The authors declare that they have no conflict of interest.

References

Bretherton, C. S., Widmann, M., Dymnikov, V. P., Wallace, J. M., and Bladé, I.: The Effective Number of Spatial Degrees of Freedom of
a Time-Varying Field, J. Climate, 12, 1990–2009, https://doi.org/10.1175/1520-0442(1999)012<1990:TENOSD>2.0.CO;2, 1999.

Brun, E., Six, D., Picard, G., Vionnet, V., Arnaud, L., Bazile, E., Boone, A., Bouchard, A., Genthon, C., Guidard, V., Moigne, P. L.,
Rabier, F., and Seity, Y.: Snow/atmosphere coupled simulation at Dome C, Antarctica, J. Glaciol., 57, 721–736,
https://doi.org/10.3189/002214311797409794, 2011.

Buizert, C., Fudge, T. J., Roberts, W. H. G., Steig, E. J., Sherriff-Tadano, S., Ritz, C., Lefebvre, E., Edwards, J., Kawamura, K., Oyabu, I.,
Motoyama, H., Kahle, E. C., Jones, T. R., Abe-Ouchi, A., Obase, T., Martin, C., Corr, H., Severinghaus, J. P., Beaudette, R.,
Epifanio, J. A., Brook, E. J., Martin, K., Chappellaz, J., Aoki, S., Nakazawa, T., Sowers, T. A., Alley, R. B., Ahn, J., Sigl, M.,
Severi, M., Dunbar, N. W., Svensson, A., Fegyveresi, J. M., He, C., Liu, Z., Zhu, J., Otto-Bliesner, B. L., Lipenkov, V. Y.,

33

Kageyama, M., and Schwander, J.: Antarctic surface temperature and elevation during the Last Glacial Maximum, Science, 372, 1097–1101, https://doi.org/10.1126/science.abd2897, 2021.

Casado, M., Landais, A., Masson-Delmotte, V., Genthon, C., Kerstel, E., Kassi, S., Arnaud, L., Picard, G., Prie, F., Cattani, O., Steen-Larsen, H.-C., Vignon, E., and Cermak, P.: Continuous measurements of isotopic composition of water vapour on the EastAntarctic Plateau, Atmos. Chem. Phys., 16, 8521–8538, https://doi.org/10.5194/acp-16-8521-2016, 2016.

Casado, M., Orsi, A., and Landais, A.: On the limits of climate reconstruction from water stable isotopes in polar ice cores, PAGES Mag, 25, 146–147, https://doi.org/10.22498/pages.25.3.146, 2017.

Casado, M., Landais, A., Picard, G., Münch, T., Laepple, T., Stenni, B., Dreossi, G., Ekaykin, A., Arnaud, L., Genthon, C., Touzeau, A., Masson-Delmotte, V., and Jouzel, J.: Archival processes of the water stable isotope signal in East Antarctic ice cores, The Cryosphere, 12, 1745–1766, https://doi.org/10.5194/tc-12-1745-2018, 2018.

Casado, M., Landais, A., Picard, G., Arnaud, L., Dreossi, G., Stenni, B., and Prié, F.: Isotopic composition of surface snow at Dome C, Antarctica in 2013-2018, PANGAEA [dataset], https://doi.org/10.1594/PANGAEA.934415, 2021a.

Casado, M., Landais, A., Picard, G., Arnaud, L., Dreossi, G., Stenni, B., and Prié, F.: Water Isotopic Signature of Surface Snow Metamorphism in Antarctica, Geophys Res Lett, 48, https://doi.org/10.1029/2021GL093382, 2021b.

Cauquoin, A. and Werner, M.: High-Resolution Nudged Isotope Modeling With ECHAM6-Wiso: Impacts of Updated Model Physics and ERA5 Reanalysis Data, J Adv Model Earth Syst, 13, https://doi.org/10.1029/2021MS002532, 2021.

Cauquoin, A. and Werner, M.: ECHAM6-wiso nudged simulation water isotopes and precipitation for the period 1990-2020, Zenodo [dataset], https://doi.org/10.5281/zenodo.8341390, 2023.

Cauquoin, A., Werner, M., and Lohmann, G.: Water isotopes – climate relationships for the mid-Holocene and preindustrial period simulated with an isotope-enabled version of MPI-ESM, Clim. Past, 15, 1913–1937, https://doi.org/10.5194/cp-15-1913-2019, 2019.

Craig, H.: Standard for Reporting Concentrations of Deuterium and Oxygen-18 in Natural Waters, Science, 133, 1833–1834, https://doi.org/10.1126/science.133.3467.1833, 1961.

Dansgaard, W.: Stable isotopes in precipitation, Tellus, 16, 436–468, https://doi.org/10.3402/tellusa.v16i4.8993, 1964.

Dietrich, L. J., Steen-Larsen, H. C., Wahl, S., Jones, T. R., Town, M. S., and Werner, M.: Snow-Atmosphere Humidity Exchange at the Ice Sheet Surface Alters Annual Mean Climate Signals in Ice Core Records, Geophysical Research Letters, 50, e2023GL104249, https://doi.org/10.1029/2023GL104249, 2023.

Dietrich, L. J., Steen-Larsen, H. C., Wahl, S., Faber, A.-K., and Fettweis, X.: On the importance of the humidity flux for the surface mass balance in the accumulation zone of the Greenland Ice Sheet, The Cryosphere, 18, 289–305, https://doi.org/10.5194/tc-18-289-2024, 2024.

Dreossi, G.: A decade (2008-2017) of water stable-isotope composition of precipitation at Concordia Station, East Antarctica, Zenodo [dataset], https://doi.org/10.5281/zenodo.10197160, 2023.

Dreossi, G., Masiol, M., Stenni, B., Zannoni, D., Scarchilli, C., Ciardini, V., Casado, M., Landais, A., Werner, M., Cauquoin, A., Casasanta, G., Del Guasta, M., Posocco, V., and Barbante, C.: A decade (2008–2017) of water stable-isotope composition of precipitation at Concordia Station, East Antarctica, Snow/Antarctic, https://doi.org/10.5194/egusphere-2023-2813, 2023.

Frezzotti, M., Pourchet, M., Flora, O., Gandolfi, S., Gay, M., Urbini, S., Vincent, C., Becagli, S., Gragnani, R., Proposito, M., Severi, M., Traversi, R., Udisti, R., and Fily, M.: Spatial and temporal variability of snow accumulation in East Antarctica from traverse data, J. Glaciol., 51, 113–124, https://doi.org/10.3189/172756505781829502, 2005.

Gallée, H. and Schayes, G.: Development of a Three-Dimensional Meso-γ Primitive Equation Model: Katabatic Winds Simulation in the Area of Terra Nova Bay, Antarctica, Monthly Weather Review, 122, 671–685, https://doi.org/10.1175/1520-0493(1994)122<0671:DOATDM>2.0.CO;2, 1994.

Genthon, C., Six, D., Scarchilli, C., Ciardini, V., and Frezzotti, M.: Meteorological and snow accumulation gradients across Dome C, East Antarctic plateau: Meteorological and snow accumulation gradients at Dome C, Int. J. Climatol., 36, 455–466, https://doi.org/10.1002/joc.4362, 2015.

Genthon, C., Piard, L., Vignon, E., Madeleine, J.-B., Casado, M., and Gallée, H.: Atmospheric moisture supersaturation in the near-surface atmosphere at Dome C, Antarctic Plateau, Atmos. Chem. Phys., 17, 691–704, https://doi.org/10.5194/acp-17-691-2017, 2017.

Genthon, C., Veron, D., Vignon, E., Six, D., Dufresne, J.-L., Madeleine, J.-B., Sultan, E., and Forget, F.: 10 years of temperature and wind observation on a 45 m tower at Dome C, East Antarctic plateau, Earth Syst. Sci. Data, 13, 5731–5746, https://doi.org/10.5194/essd-13-5731-2021, 2021a.

Genthon, C., Veron, D., Vignon, E., Six, D., Dufresne, J. L., Madeleine, J.-B., Sultan, E., and Forget, F.: Ten years of shielded ventilated atmospheric temperature observation on a 45-m tower at Dome C, East Antarctic plateau, PANGAEA [dataset], https://doi.org/10.1594/PANGAEA.932512, 2021b.

Genthon, C., Veron, D., Vignon, E., Six, D., Dufresne, J. L., Madeleine, J.-B., Sultan, E., and Forget, F.: Ten years of wind speed observation on a 45-m tower at Dome C, East Antarctic plateau, PANGAEA [dataset], https://doi.org/10.1594/PANGAEA.932513, 2021c.

Genthon, C., Veron, D., Vignon, E., Madeleine, J.-B., and Piard, L.: Water vapor observation at 3 m height above ground at Dome C, East Antarctic plateau (2018-2020), PANGAEA [dataset], https://doi.org/10.1594/PANGAEA.939421, 2021d.

Genthon, C., Veron, D. E., Vignon, E., Madeleine, J.-B., and Piard, L.: Water vapor in cold and clean atmosphere: a 3-year data set in the boundary layer of Dome C, East Antarctic Plateau, Earth Syst. Sci. Data, 14, 1571–1580, https://doi.org/10.5194/essd-14-1571-2022, 2022.

Gkinis, V., Simonsen, S. B., Buchardt, S. L., White, J. W. C., and Vinther, B. M.: Water isotope diffusion rates from the NorthGRIP ice core for the last 16,000 years – Glaciological and paleoclimatic implications, Earth and Planetary Science Letters, 405, 132–141, https://doi.org/10.1016/j.epsl.2014.08.022, 2014.

Gonfiantini, R.: Standards for stable isotope measurements in natural compounds, Nature, 271, 534–536, https://doi.org/10.1038/271534a0, 1978.

Grachev, A. A., Andreas, E. L., Fairall, C. W., Guest, P. S., and Persson, P. O. G.: SHEBA flux–profile relationships in the stable atmospheric boundary layer, Boundary-Layer Meteorol, 124, 315–333, https://doi.org/10.1007/s10546-007-9177-6, 2007.

Grigioni, P., Camporeale, G., Ciardini, V., De Silvestri, L., Iaccarino, A., Proposito, M., and Scarchilli, C.: Dati meteorologici della Stazione meteorologica CONCORDIA presso la Base CONCORDIA STATION (Dome C), ENEA [dataset], https://doi.org/10.12910/DATASET2022-002, 2022.

Harris Stuart, R., Faber, A.-K., Wahl, S., Hörhold, M., Kipfstuhl, S., Vasskog, K., Behrens, M., Zuhr, A. M., and Steen-Larsen, H. C.: Exploring the role of snow metamorphism on the isotopic composition of the surface snow at EastGRIP, The Cryosphere, 17, 1185–1204, https://doi.org/10.5194/tc-17-1185-2023, 2023.

Hersbach, H., Bell, B., Berrisford, P., Hirahara, S., Horányi, A., Muñoz-Sabater, J., Nicolas, J., Peubey, C., Radu, R., Schepers, D., Simmons, A., Soci, C., Abdalla, S., Abellan, X., Balsamo, G., Bechtold, P., Biavati, G., Bidlot, J., Bonavita, M., De Chiara, G., Dahlgren, P., Dee, D., Diamantakis, M., Dragani, R., Flemming, J., Forbes, R., Fuentes, M., Geer, A., Haimberger, L., Healy, S.,

Hogan, R. J., Hólm, E., Janisková, M., Keeley, S., Laloyaux, P., Lopez, P., Lupu, C., Radnoti, G., De Rosnay, P., Rozum, I., Vamborg, F., Villaume, S., and Thépaut, J.: The ERA5 global reanalysis, Quart J Royal Meteoro Soc, 146, 1999–2049, https://doi.org/10.1002/qj.3803, 2020.

Högström, U.: Review of some basic characteristics of the atmospheric surface layer, Boundary-Layer Meteorology, 78, 215–246, 1996.

995   Holtslag, A. A. M. and De Bruin, H. A. R.: Applied Modeling of the Nighttime Surface Energy Balance over Land, J. Appl. Meteor., 27, 689–704, https://doi.org/10.1175/1520-0450(1988)027<0689:AMOTNS>2.0.CO;2, 1988.

Hughes, A. G., Wahl, S., Jones, T. R., Zuhr, A., Hörhold, M., White, J. W. C., and Steen-Larsen, H. C.: The role of sublimation as a driver of climate signals in the water isotope content of surface snow: laboratory and field experimental results, The Cryosphere, 15, 4949–4974, https://doi.org/10.5194/tc-15-4949-2021, 2021.

1000   Johnsen, S. J., Clausen, H. B., Cuffey, K. M., Hoffmann, G., Schwander, J., and Creyts, T.: Diffusion of stable isotopes in polar firn and ice: the isotope effect in firn diffusion, Physics of Ice Core Records, 121–140, https://doi.org/10.7916/D8KW5D4X, 2000.

Jouzel, J., Merlivat, L., and Lorius, C.: Deuterium excess in an East Antarctic ice core suggests higher relative humidity at the oceanic surface during the last glacial maximum, Nature, 299, 688–691, https://doi.org/10.1038/299688a0, 1982.

Jouzel, J. and Merlivat, L.: Deuterium and Oxygen 18 in Precipitation: Modeling of the Isotopic Effects During Snow Formation, J. Geophys. Res, 89, 11749-11757, https://doi.org/10.1029/JD089iD07p11749, 1984.

1005   King, J. C. and Anderson, P. S.: Heat and water vapour fluxes and scalar roughness lengths over an Antarctic ice shelf, Boundary-Layer Meteorol, 69, 101–121, https://doi.org/10.1007/BF00713297, 1994.

King, J. C., Anderson, P. S., and Mann, G. W.: The seasonal cycle of sublimation at Halley, Antarctica, J. Glaciol., 47, 1–8, https://doi.org/10.3189/172756501781832548, 2001.

1010   Kino, K., Okazaki, A., Cauquoin, A., and Yoshimura, K.: Contribution of the Southern Annular Mode to Variations in Water Isotopes of Daily Precipitation at Dome Fuji, East Antarctica, JGR Atmospheres, 126, e2021JD035397, https://doi.org/10.1029/2021JD035397, 2021.

Kopec, B. G., Feng, X., Posmentier, E. S., and Sonder, L. J.: Seasonal Deuterium Excess Variations of Precipitation at Summit, Greenland, and their Climatological Significance, JGR Atmospheres, 124, 72–91, https://doi.org/10.1029/2018JD028750, 2019.

1015   Landais, A., Stenni, B., Masson-Delmotte, V., Jouzel, J., Cauquoin, A., Fourré, E., Minster, B., Selmo, E., Extier, T., Werner, M., Vimeux, F., Uemura, R., Crotti, I., and Grisart, A.: Interglacial Antarctic–Southern Ocean climate decoupling due to moisture source area shifts, Nat. Geosci., 14, 918–923, https://doi.org/10.1038/s41561-021-00856-4, 2021.

Leduc-Leballeur, M., Picard, G., Macelloni, G., Arnaud, L., Brogioni, M., Mialon, A., and Kerr, Y. H.: Influence of snow surface properties on L-band brightness temperature at Dome C, Antarctica, Remote Sensing of Environment, 199, 427–436, 1020   https://doi.org/10.1016/j.rse.2017.07.035, 2017.

Lettau, H. H.: Wind and temperature profile prediction for diabatic surface layers including strong inversion cases, Boundary-Layer Meteorol 17, 443–464, https://doi.org/10.1007/BF00118610, 1979.

Libois, Q., Picard, G., Arnaud, L., Morin, S., and Brun, E.: Modeling the impact of snow drift on the decameter-scale variability of snow properties on the Antarctic Plateau, J. Geophys. Res. Atmos., 119, 11,662-11,681, https://doi.org/10.1002/2014JD022361, 2014.

1025   Lorius, C. and Merlivat, L.: Distribution of mean surface stable isotopes values in East Antarctica; Observed changes with depth in coastal area, General Assembly of the International Union of Geodesy and Geophysics, 1975.

Lorius, C., Merlivat, L., and Hagemann, R.: Variation in the mean deuterium content of precipitations in Antarctica, J. Geophys. Res., 74, 7027–7031, https://doi.org/10.1029/JC074i028p07027, 1969.

Lupi, A., Lanconelli, C., and Vitale, V.: Basic and other measurements of radiation at Concordia station (2006-01 et seq), PANGAEA
1030   [dataset], https://doi.org/10.1594/PANGAEA.935421, 2021.

Masson-Delmotte, V., Landais, A., Stievenard, M., Cattani, O., Falourd, S., Jouzel, J., Johnsen, S. J., Dahl-Jensen, D., Sveinsbjornsdottir,
A., White, J. W. C., Popp, T., and Fischer, H.: Holocene climatic changes in Greenland: Different deuterium excess signals at
Greenland Ice Core Project (GRIP) and NorthGRIP, J. Geophys. Res., 110, 2004JD005575,
https://doi.org/10.1594/PANGAEA.935421, 2005.

1035 Masson-Delmotte, V., Hou, S., Ekaykin, A., Jouzel, J., Aristarain, A., Bernardo, R. T., Bromwich, D., Cattani, O., Delmotte, M., Falourd,
S., Frezzotti, M., Gallée, H., Genoni, L., Isaksson, E., Landais, A., Helsen, M. M., Hoffmann, G., Lopez, J., Morgan, V., Motoyama,
H., Noone, D., Oerter, H., Petit, J. R., Royer, A., Uemura, R., Schmidt, G. A., Schlosser, E., Simões, J. C., Steig, E. J., Stenni, B.,
Stievenard, M., van den Broeke, M. R., van de Wal, R. S. W., van de Berg, W. J., Vimeux, F., and White, J. W. C.: A Review of
Antarctic Surface Snow Isotopic Composition: Observations, Atmospheric Circulation, and Isotopic Modeling*, Journal of Climate,
1040   21, 3359–3387, https://doi.org/10.1175/2007JCLI2139.1, 2008.

Merlivat, L. and Jouzel, J.: Global climatic interpretation of the deuterium-oxygen 18 relationship for precipitation, J. Geophys. Res., 84,
5029–5033, https://doi.org/10.1029/JC084iC08p05029, 1979.

Monin, A. S. and Obukhov, A. M.: Basic laws of turbulent mixing in the surface layer of the atmosphere, Trudy Geofiz Inst, 24, 163–187,
1954.

1045 Münch, T., Kipfstuhl, S., Freitag, J., Meyer, H., and Laepple, T.: Constraints on post-depositional isotope modifications in East Antarctic
firn from analysing temporal changes of isotope profiles, The Cryosphere, 11, 2175–2188, https://doi.org/10.5194/tc-11-2175-2017,
2017.

Muñoz Sabater, J.: ERA5-Land hourly data from 1950 to present, Copernicus Climate Change Service (C3S) Climate Data Store (CDS)
[dataset], https://doi.org/10.24381/cds.e2161bac, 2019.

1050 Murphy, D. M. and Koop, T.: Review of the vapour pressures of ice and supercooled water for atmospheric applications, Q. J. R.
Meteorol. Soc., 131, 1539–1565, https://doi.org/10.1256/qj.04.94, 2005.

Picard, G., Royer, A., Arnaud, L., and Fily, M.: Influence of meter-scale wind-formed features on the variability of the microwave
brightness temperature around Dome C in Antarctica, The Cryosphere, 8, 1105–1119, https://doi.org/10.5194/tc-8-1105-2014, 2014.

Picard, G., Arnaud, L., Caneill, R., Lefebvre, E., and Lamare, M.: Observation of the process of snow accumulation on the Antarctic
1055   Plateau by time lapse laser scanning, The Cryosphere, 13, 1983–1999, https://doi.org/10.5194/tc-13-1983-2019, 2019.

Risi, C., Landais, A., Winkler, R., and Vimeux, F.: Can we determine what controls the spatio-temporal distribution of d-excess and 17O-
excess in precipitation using the LMDZ general circulation model?, Clim. Past, 9, 2173–2193, https://doi.org/10.5194/cp-9-2173-
2013, 2013.

Servettaz, A. P. M., Agosta, C., Kittel, C., and Orsi, A. J.: Control of the temperature signal in Antarctic proxies by snowfall dynamics,
1060   The Cryosphere, 17, 5373–5389, https://doi.org/10.5194/tc-17-5373-2023, 2023.

Steen-Larsen, H. C., Masson-Delmotte, V., Sjolte, J., Johnsen, S. J., Vinther, B. M., Bréon, F.-M., Clausen, H. B., Dahl-Jensen, D.,
Falourd, S., Fettweis, X., Gallée, H., Jouzel, J., Kageyama, M., Lerche, H., Minster, B., Picard, G., Punge, H. J., Risi, C., Salas, D.,
Schwander, J., Steffen, K., Sveinbjörnsdóttir, A. E., Svensson, A., and White, J.: Understanding the climatic signal in the water
stable isotope records from the NEEM shallow firn/ice cores in northwest Greenland, J. Geophys. Res., 116, D06108,
1065   https://doi.org/10.1029/2010JD014311, 2011.

Steen-Larsen, H. C., Sveinbjörnsdottir, A. E., Peters, A. J., Masson-Delmotte, V., Guishard, M. P., Hsiao, G., Jouzel, J., Noone, D., Warren, J. K., and White, J. W. C.: Climatic controls on water vapor deuterium excess in the marine boundary layer of the North Atlantic based on 500 days of in situ, continuous measurements, Atmos. Chem. Phys., 14, 7741–7756, https://doi.org/10.5194/acp-14-7741-2014, 2014a.

1070 Steen-Larsen, H. C., Masson-Delmotte, V., Hirabayashi, M., Winkler, R., Satow, K., Prié, F., Bayou, N., Brun, E., Cuffey, K. M., Dahl-Jensen, D., Dumont, M., Guillevic, M., Kipfstuhl, S., Landais, A., Popp, T., Risi, C., Steffen, K., Stenni, B., and Sveinbjörnsdottír, A. E.: What controls the isotopic composition of Greenland surface snow?, Clim. Past, 10, 377–392, https://doi.org/10.5194/cp-10-377-2014, 2014b.

Stenni, B., Masson-Delmotte, V., Johnsen, S., Jouzel, J., Longinelli, A., Monnin, E., Röthlisberger, R., and Selmo, E.: An Oceanic Cold
1075 Reversal During the Last Deglaciation, Science, 293, 2074–2077, https://doi.org/10.1126/science.1059702, 2001.

Stenni, B., Scarchilli, C., Masson-Delmotte, V., Schlosser, E., Ciardini, V., Dreossi, G., Grigioni, P., Bonazza, M., Cagnati, A., Karlicek, D., Risi, C., Udisti, R., and Valt, M.: Three-year monitoring of stable isotopes of precipitation at Concordia Station, East Antarctica, The Cryosphere, 10, 2415–2428, https://doi.org/10.5194/tc-10-2415-2016, 2016.

Touzeau, A., Landais, A., Stenni, B., Uemura, R., Fukui, K., Fujita, S., Guilbaud, S., Ekaykin, A., Casado, M., Barkan, E., Luz, B.,
1080 Magand, O., Teste, G., Le Meur, E., Baroni, M., Savarino, J., Bourgeois, I., and Risi, C.: Acquisition of isotopic composition for surface snow in East Antarctica and the links to climatic parameters, The Cryosphere, 10, 837–852, https://doi.org/10.5194/tc-10-837-2016, 2016.

Town, M. S., Warren, S. G., Walden, V. P., and Waddington, E. D.: Effect of atmospheric water vapor on modification of stable isotopes in near-surface snow on ice sheets, J. Geophys. Res., 113, 2008JD009852, https://doi.org/10.1029/2008JD009852, 2008.

1085 Uemura, R., Matsui, Y., Yoshimura, K., Motoyama, H., and Yoshida, N.: Evidence of deuterium excess in water vapor as an indicator of ocean surface conditions, J. Geophys. Res., 113, 2008JD010209, https://doi.org/10.1029/2008JD010209, 2008.

Uemura, R., Masson-Delmotte, V., Jouzel, J., Landais, A., Motoyama, H., and Stenni, B.: Ranges of moisture-source temperature estimated from Antarctic ice cores stable isotope records over glacial–interglacial cycles, Clim. Past, 8, 1109–1125, https://doi.org/10.5194/cp-8-1109-2012, 2012.

1090 Vignon, E., Genthon, C., Barral, H., Amory, C., Picard, G., Gallée, H., Casasanta, G., and Argentini, S.: Momentum- and Heat-Flux Parametrization at Dome C, Antarctica: A Sensitivity Study, Boundary-Layer Meteorol, 162, 341–367, https://doi.org/10.1007/s10546-016-0192-3, 2016.

Vignon, E., Raillard, L., Genthon, C., Del Guasta, M., Heymsfield, A. J., Madeleine, J.-B., and Berne, A.: Ice fog observed at cirrus temperatures at Dome C, Antarctic Plateau, Atmos. Chem. Phys., 22, 12857–12872, https://doi.org/10.5194/acp-22-12857-2022,
1095 2022.

Vimeux, F., Masson, V., Jouzel, J., Stievenard, M., and Petit, J. R.: Glacial–interglacial changes in ocean surface conditions in the Southern Hemisphere, Nature, 398, 410–413, https://doi.org/10.1038/18860, 1999.

Wahl, S., Steen-Larsen, H. C., Reuder, J., and Hörhold, M.: Quantifying the Stable Water Isotopologue Exchange Between the Snow Surface and Lower Atmosphere by Direct Flux Measurements, JGR Atmospheres, 126, e2020JD034400,
1100 https://doi.org/10.1029/2020JD034400, 2021.

Wahl, S., Steen-Larsen, H. C., Hughes, A. G., Dietrich, L. J., Zuhr, A., Behrens, M., Faber, A. -K., and Hörhold, M.: Atmosphere-Snow Exchange Explains Surface Snow Isotope Variability, Geophysical Research Letters, 49, https://doi.org/10.1029/2022GL099529, 2022.

Werner, M., Jouzel, J., Masson-Delmotte, V., and Lohmann, G.: Reconciling glacial Antarctic water stable isotopes with ice sheet
1105   topography and the isotopic paleothermometer, Nat Commun, 9, 3537, https://doi.org/10.1038/s41467-018-05430-y, 2018.

Zuhr, A. M., Münch, T., Steen-Larsen, H. C., Hörhold, M., and Laepple, T.: Local-scale deposition of surface snow on the Greenland ice
       sheet, The Cryosphere, 15, 4873–4900, https://doi.org/10.5194/tc-15-4873-2021, 2021.

Zuhr, A. M., Wahl, S., Steen-Larsen, H. C., Hörhold, M., Meyer, H., and Laepple, T.: A Snapshot on the Buildup of the Stable Water
       Isotopic Signal in the Upper Snowpack at EastGRIP on the Greenland Ice Sheet, JGR Earth Surface, 128, e2022JF006767,
1110   https://doi.org/10.1029/2022JF006767, 2023.